PERGAMON

International Journal of Solids and Structures 37 (2000) 1841–1871

INTERNATIONAL JOURNAL OF SOLIDS and STRUCTURES

www.elsevier.com/locate/ijsolstr

Mechanical and numerical modeling of a porous elastic–viscoplastic material with tensile failure

M.B. Rubin[a,*], O.Yu. Vorobiev[b], L.A. Glenn[b]

[a]*Faculty of Mechanical Engineering, Technion—Israel Institute of Technology, 32000 Haifa, Israel*
[b]*Geophysics and Global Security Division, Lawrence Livermore National Laboratory, Livermore, CA 94550, USA*

Received 7 April 1998; in revised form 12 November 1998

Abstract

The objective of this paper is to develop simple but comprehensive constitutive equations that model a number of physical phenomena exhibited by dry porous geological materials and metals. For geological materials the equations model: porous compaction; porous dilation due to distortional deformation and tensile failure; shear enhanced compaction; pressure hardening of the yield strength; damage of the yield strength due to distortional deformation and porosity changes; and dependence of the yield strength on the Lode angle. For metals the equations model: hardening of the yield strength due to plastic deformation; pressure and temperature dependence of the yield strength, and damage due to nucleation of porosity during tensile failure. The equations are valid for large deformations and the elastic response is hyperelastic in the sense that the stress is related to a derivative of the Helmholtz free energy. Also, the equations are viscoplastic with rate dependence occurring in both the evolution equations of porosity and elastic distortional deformations. Moreover, formulas are presented for robust numerical integration of the evolution equations at the element level that can be easily implemented into standard computer programs for dynamic response of materials.

Keywords: Failure; Finite deformation; Plasticity; Porous media; Viscoplastic

1. Introduction

Developing realistic mathematical constitutive equations to model the dynamic response of a wide range of materials has been a main objective of research in continuum mechanics for the last few decades. With ever increasing computational power of modern computers it has become more practical to implement these nonlinear constitutive equations in real applications. The response of structures to

* Corresponding author. Fax: 00 972 4 832 4533.
E-mail address: mbrubin@tx.technion.ac.il (M.B. Rubin)

0020-7683/00/$ - see front matter
PII: S0020-7683(98)00333-3

Nomenclature

a, a_0, a_1, a_2	auxiliary functions controlling dependence of the yield strength on the Lode angle
A_1	material constant controlling pressure sensitivity of the shear modulus
A_2	material constant controlling temperature sensitivity of the shear modulus
A_p	rate of inelastic volume change
$\mathbf{A}_p$	rate of inelastic distortional deformation
A'	material constant controlling the rate sensitivity of inelastic deformation
b, b_0, b_1, b_2	auxiliary functions controlling dependence of the yield strength on the Lode angle
b_s	material constant that specifies the volume dependence of the Gruneisen gamma
$\mathbf{B_e}$	elastic deformation tensor
$\mathbf{B}'_\mathbf{e}$	elastic distortional deformation tensor
$\mathbf{B}'^{*}_\mathbf{e}$	elastic trial value of $\mathbf{B}'_\mathbf{e}$
$\mathbf{B}''_\mathbf{e}$	deviatoric part of the elastic distortional deformation
$\mathbf{B}''^{*}_\mathbf{e}$	elastic trial value of $\mathbf{B}''_\mathbf{e}$
c_{sv}	specific heat of the solid
c_1, c_2	material constants controlling porous compaction
c_3, c_4	material constants defining shear enhanced compaction
C_{s0}	low pressure shock velocity
d_0, d_1, d_2	auxiliary functions for the determination of the rate sensitivity of plasticity
$\mathrm{d}v$	element of total volume in the present configuration
$\mathrm{d}v_p$	element of pore volume in the present configuration
$\mathrm{d}v_s$	element of solid volume in the present configuration
$\mathrm{d}V$	element of total volume in the reference configuration
$\mathrm{d}V_p$	element of pore volume in the reference configuration
$\mathrm{d}V_s$	element of solid volume in the reference configuration
D	shock velocity
D_u	uniaxial deformation rate
D_v	dilatational deformation rate
$\mathbf{D}$	rate of deformation tensor, symmetric part of $\mathbf{L}$
$\mathbf{D_p}$	rate of plastic deformation
e_v	elastic volume strain
$\mathbf{e}_i$	rectangular Cartesian base vectors
E_{11}	Lagrangian axial strain
E_{12}	Lagrangian shear strain
E_v	Lagrangian volumetric strain
f	function that controls the effect of damage
f_1, f_2	functions defining the Helmholtz free energy
F_1	function that controls hardening of the yield strength
F_2	function that controls pressure sensitivity of the yield strength
F_3	function that controls damage of the yield strength due to distortional deformation
F_4	function that controls dependence of the yield strength on the Lode angle
F_5	function that controls the dependence of the yield strength on pressure and temperature
F_6	function that controls dependence of the yield strength on porosity
F_7	function that controls damage of the yield strength due to porosity changes

F_8	function that controls shear enhanced compaction
$\boldsymbol{F} = \partial\mathbf{x}/\partial\mathbf{X}$	the total deformation gradient
g	yield function
G	shear modulus
G_0	value of the shear modulus in the reference configuration
$\mathbf{g}$	temperature gradient relative to the present configuration
$\mathbf{g}'_e$	elastic distortional strain
$H(x)$	Heaviside function
$\mathbf{I}$	second-order unity tensor
J	total relative volume
J_c	total relative volume at the onset of porous compaction
J_e	elastic relative volume
J_s	relative volume of the solid
k	heat conduction coefficient
K	material constant for plastic strain hardening
k_1, k_2	material constants defining the function F_1
k_3, k_4	material constants defining the function F_2
k_5, k_6	material constants defining the function F_3
k_7, k_8	material constants defining damage due to porosity on Y and p_d
$\mathbf{L}$	velocity gradient
m	material constant controlling the rate dependence of porous dilation on spall strength
m_d	material constant controlling the rate of porous dilatation due to distortional deformation
n	material constant controlling the shape of the spall curve
p	total pressure
p^*	material constant controlling the rate of porous dilatation due to distortional deformation
p_c	value of the pressure at the onset of porous compaction
p_d	function controlling the magnitude of the pressure during porous dilation
p_{d0}	material constant that controls the negative value of pressure at the onset of porous dilation
p_s	pressure in the solid
p_{sl}	pressure in the solid mainly due to volume and temperature
p'_s	pressure in the solid mainly due to elastic distortional deformation
p_{sH}	pressure on the Hugoniot
$\mathbf{p}$	external rate of entropy flux per unit present area
q	material constant that controls the transition from Mohr–Coulomb to Mises response
Q_1, Q_{10}	functions that control the yield strength during torsion (TOR)
Q_2, Q_{20}	functions that control the yield strength during triaxial extension (TXE)
Q	function that controls the transition from Mohr–Coulomb to Mises response
$\mathbf{q}$	external rate of heat flux per unit present area
r	specific external rate of heat supply
s	specific external rate of supply entropy
S_1, S_2, S_3	material constants that specify the shock velocity vs particle velocity curve
t	time
t_1	beginning of a time step

t_2	end of a time step
$\mathbf{T}$	Cauchy stress tensor
$\mathbf{T}'$	deviatoric part of the Cauchy stress
$\mathbf{T}'^*$	elastic trial value of $\mathbf{T}'$
$\mathbf{T}'_s$	deviatoric part of the Cauchy stress in the solid
$\mathbf{v}$	velocity of a material point
x_i	rectangular Cartesian components of $\mathbf{x}$
X_A	rectangular Cartesian components of $\mathbf{X}$
$\mathbf{x}$	position vector of a material point in the present configuration
$\mathbf{X}$	position vector of a material point in the reference configuration
Y	yield strength in uniaxial stress
Y^*	elastic trial value of Y
Y_0	reference value of the yield strength
Y'_1	maximum value of the yield strength due to plastic strain hardening
$\langle x \rangle$	McAuley brackets

Greek symbols

α_1	invariant of elastic distortional deformation
α_2	invariant of elastic distortional deformation
β	Lode angle
γ_s	Gruneisen gamma for the solid in the present configuration
γ_{s0}	Gruneisen gamma for the solid in the reference configuration
Γ_d	material constant controlling the rate of porous dilation
Γ_c	material constant controlling porous compaction
Γ_p	function controlling the magnitude of elastic distortional deformation
Γ_{p0}	material constant controlling the rate sensitivity of inelastic deformation
Δt	time interval
ε	specific internal energy
ε_d	material constant controlling damage due to distortional deformation
ε_p	equivalent plastic strain
ε_{sl}	specific energy of the solid mainly due to volume and temperature
ε'_s	specific energy of the solid mainly due to elastic distortional deformation
ε_{sH}	specific internal energy on the Hugoniot
ε_v	material constant controlling the rate of damage due to porous compaction
η	entropy per unit mass
η_s	specific entropy of the solid
η_{sl}	specific entropy of the solid mainly due to volume and temperature
η'_s	specific entropy of the solid mainly due to elastic distortional deformation
θ	absolute temperature
θ_0	value of θ in the reference configuration
κ	rate of shearing
λ	scalar controlling the amount of radial return of the stress due to plasticity
$\bar{\lambda}$	auxiliary variable for determination of rate sensitivity of plasticity
ν	Poisson's ratio
ξ	specific internal rate of production of entropy
ξ'	specific internal rate of entropy production due to material dissipation

ξ'_{d}	specific internal rate of entropy production due to inelastic distortional deformation
ξ'_{ϕ}	specific internal rate of entropy production due to porosity changes
ρ	mass per unit present total volume
ρ_0	mass per unit reference total volume
ρ_{s}	mass of the solid per unit present solid volume
ρ_{s0}	mass of the solid per unit reference solid volume
σ^*	spall stress
σ_{e}	von Mises effective stress
σ^*_{e}	elastic trial value of σ_{e}
Φ	porosity in the reference configuration
ϕ	porosity in the present configuration
$\phi_{\min}$	minimum value of porosity attained during loading
$\phi_{\max}$	maximum value of porosity attained during loading
ϕ^*	material constant controlling the amount of porous dilatation due to distortional deformation
$\phi^*_{\min}$	minimum value of $\phi_{\min}$ and ϕ^*
ϕ^*_{c}	maximum value of ϕ^{**}_c and ϕ^*
ϕ^{**}_{c}	function controlling porous compaction
ϕ^*_{d}	function controlling the amount of porous dilation
ϕ_{s}	material constant related to the spall strain
ψ	specific Helmholtz free energy
ψ_{s}	specific Helmholtz free energy of the solid
ψ_{sl}	specific Helmholtz free energy of the solid mainly due to volume and temperature
ω	measure of damage due to porosity changes
Ω	measure of damage due to distortional deformation

shock loading is a particularly challenging area of research. Near the source of the shock loading it is necessary to model fully coupled nonlinear thermomechanical effects. In that region, the magnitude of the deviatoric stress is usually much smaller than that of the pressure so details of the strength of the material being loaded are often negligible. However, due to the divergent effect of spherical geometry these strength effects become quite significant as the shock wave propagates away from the source and approaches free surfaces or buried structures. Thus, it is necessary to use thermodynamically consistent constitutive equations for nonlinear deformations that are applicable both near the source and far away from it.

It is well known that when metals experiences sufficient distortion, dislocations tend to move through the atomic lattice causing macroscopic plastic deformations. Also, when metals are subjected to sufficient tension then voids tend to initiate and grow causing tensile failure. Such effects can usually be modeled using a yield function that limits the value of von Mises stress by a yield strength which depends on a hardening variable, by introducing a measure of porosity to model void growth, and by introducing a measure of damage that reduces the yield strength due to tensile failure. Geological materials differ from metals in that inelastic deformations are not due to motions of dislocations but rather due to damage associated with microfracturing and granular flow. Nevertheless, the mathematical structure of plasticity theory seems to be capable of capturing the main features of the response of these materials as well. Therefore, in this paper the term plasticity will be used in a general sense to include all inelastic deformation.

In modeling geological materials the yield strength depends on both pressure and the Lode angle (e.g. Hill, 1950, p. 18). Also, porosity in these materials is naturally due to their granular nature and it measures not only voids but microcracks as well. At sufficient levels of pressure, compaction occurs and the porosity decreases. Moreover, shear enhanced compaction can occur when both pressure and deviatoric stress are acting simultaneously. Porous dilation with increasing porosity occurs during tensile failure and can also occur when damage is caused by inelastic distortional deformation. In addition, both metals and geological materials can exhibit strain-rate sensitivity.

The experimental data for geological materials often exhibit significant scatter due to natural inhomogeneity and size dependence of the samples being tested. In this paper analytical forms are specified for constitutive functions that attempt to model the main effects observed. However, it is also possible to specify many of these functions in tabular form for more flexibility in accurately modeling specific experimental data.

Furthermore, since metals become porous when ductile failure occurs with void growth, the theoretical structure for modeling porosity in geological materials can be used for metals as well. Similarly, the theoretical structure for plasticity in metals (where the von Mises stress is limited by a yield stress) is valid for geological materials as well, with the yield stress being a function of different physical phenomena for each material. Consequently, the objective of the present paper is to present rather simple comprehensive constitutive equations that model all of the above mentioned physical phenomena for metals and geological materials. In particular, the present constitutive equations collect together features of a number of models that have been presented in the literature. Various compromises are always implemented in the development of a specific constitutive equation. Here, an attempt is made to introduce specific modifications of these constitutive equations that make minor alterations in the predicted material response but make major improvements in the robustness of the associated approximate numerical solutions.

For example, constitutive equations are often formulated in terms of yield, compaction and dilation surfaces which are algebraic constraints on various parameters. Such constraints can be difficult to solve simultaneously and can also lead to numerical stiffness. Here, instead of proposing a compaction surface to determine the value of porosity, the porosity is determined by a rate-dependent evolution equation that forces the porosity to follow a specified functional form. This functional form is chosen to simulate the main features exhibited by the solution of the compaction surface formulation. However, due to the simple structure of the evolution equation, the approximate numerical solution becomes quite robust.

The constitutive equations developed in this paper are fully nonlinear, they are thermodynamically consistent, and they are properly invariant under superposed rigid body motions. They model elastically isotropic response (with respect to a stress-free reference configuration) of elastic–viscoplastic materials that can have evacuated pores, either initially or due to microfracturing. Moreover, the elastic response is hyperelastic in the sense that the Cauchy stress is related to derivatives of the Helmholtz free energy. The equations model a large range of material response exhibited by both metals and geological materials. Also, numerical algorithms are presented that determine the material response at the element level and which can easily be implemented in standard computer programs for dynamic response of materials.

An outline of the paper is as follows. Section 2 reviews the basic equations of thermodynamics of continuous media and Section 3 presents the constitutive equations for the evolution of elastic distortional deformation including the relaxation effects of viscoplasticity. Section 4 presents the evolution equations for porous dilation and compaction and Section 5 discusses the numerical integration of these evolution equations at the element level. Finally, Section 6 presents examples which exhibit the main features of the range of material response predicted by these constitutive equations.

Throughout the paper bold faced symbols are used to denote tensors and $\mathbf{I}$ denotes the second-order unit tensor. Also, $\boldsymbol{a}\cdot\boldsymbol{b}$ denotes the usual scalar product of two vectors $\mathbf{a}$, $\mathbf{b}$ and $\boldsymbol{A}\cdot\boldsymbol{B} = \mathrm{tr}\,(\mathbf{A}\mathbf{B}^{\mathrm{T}})$

denotes the scalar product of two second-order tensors $\mathbf{A}$, $\mathbf{B}$. Moreover, $\mathbf{B}^{\mathrm{T}}$ denotes the transpose of $\mathbf{B}$, $\mathrm{tr}\,\boldsymbol{A} = \boldsymbol{A} \cdot \boldsymbol{I}$ denotes the trace operation, $\det(\mathbf{A})$ denotes the determinant of the tensor $\mathbf{A}$, and the symbol $\otimes$ denotes the tensor product operator.

2. Basic equations

By way of background it is recalled that $\mathbf{X}$ denotes the location of a material point in a fixed reference configuration, $\mathbf{x}$ denotes the location of the same material point in the deformed present configuration at time t, $\mathbf{v} = \dot{\mathbf{x}}$ denotes the absolute velocity of the material point, and $\mathbf{L} = \partial \mathbf{v}/\partial \mathbf{x}$ denotes the velocity gradient. Here, and throughout the text a superposed dot is used to denote material time differentiation holding $\mathbf{X}$ fixed.

The constitutive equations are developed using the thermodynamical procedures proposed by Green and Naghdi (1977, 1978). Within this context, the usual laws of conservation of mass and balances of linear momentum, angular momentum and energy are supplemented by a balance of entropy which in local form is written as

$$\rho\dot{\eta} = \rho(s + \xi) - \mathrm{div}\,\mathbf{p}, \tag{2.1}$$

where ρ is the mass per unit present volume, η is the specific (per unit mass) entropy, s is the specific external rate of supply of entropy, ξ is the specific rate of internal production of entropy, $\mathbf{p}$ is the entropy flux per unit present surface area, and div denotes the divergence operator in the present position $\mathbf{x}$. Also, it is recalled that s and $\mathbf{p}$ are related to the absolute temperature θ, the specific external rate of heat supply r, and the heat flux vector $\mathbf{q}$ that appear in the energy equation by the expressions

$$s = \frac{r}{\theta}, \quad \mathbf{p} = \frac{\mathbf{q}}{\theta}. \tag{2.2}$$

In general, ξ can be separated into two parts

$$\rho\theta\xi = -\mathbf{p} \cdot \mathbf{g} + \rho\theta\xi', \tag{2.3}$$

where $\mathbf{g} = \partial\theta/\partial\mathbf{x}$ is the temperature gradient with respect to the present position. One part $(-\mathbf{p} \cdot \mathbf{g})$ is related to the entropy production due to heat conduction and the other part $(\rho\theta\xi')$ is related to the entropy production due to material dissipation (Rubin, 1986).

Using (2.1)–(2.3) the rate of heat supplied to the body can be written in the form

$$\rho r - \mathrm{div}\,\mathbf{q} = \rho\theta\dot{\eta} - \rho\theta\xi'. \tag{2.4}$$

Thus, the local form of the balance of energy can be expressed as

$$\rho\left(\dot{\psi} + \eta\dot{\theta}\right) - \mathbf{T} \cdot \mathbf{D} + \rho\theta\xi' = 0 \tag{2.5}$$

where the specific Helmholtz free energy ψ and the specific internal energy ε are related by the expression

$$\psi = \varepsilon - \theta\eta. \tag{2.6}$$

Also, $\mathbf{T}$ is the Cauchy stress tensor and $\mathbf{D}$ is the symmetric part of the velocity gradient $\mathbf{L}$.

Constitutive assumptions for the quantities

$$\left\{\psi, \eta, \varepsilon, \mathbf{T}, \mathbf{p}, \xi'\right\}, \tag{2.7}$$

are restricted by the usual invariance conditions under superposed rigid body motions and by the requirements that the balance of angular momentum

$$\mathbf{T}^{\mathrm{T}} = \mathbf{T}, \tag{2.8}$$

and the balance of energy (2.5) be satisfied for all thermomechanical processes. Furthermore, these constitutive equations are required to satisfy statements of the second law of thermodynamics which include the condition that heat flows from hot to cold

$$-\mathbf{p}\cdot\mathbf{g} > 0 \quad \text{for } \mathbf{g} \neq 0, \tag{2.9}$$

and the condition that the material dissipation is non-negative

$$\rho\theta\xi' \geqslant 0. \tag{2.10}$$

Instead of introducing a measure of plastic deformation and a definition of elastic deformation in terms of total and plastic deformations, it is possible to follow the work of Eckart (1948), Besseling (1966), Leonov (1976), and Rubin (1996) and introduce elastic deformation as a primary quantity which is determined by an evolution equation. In particular, here, it suffices to consider elastically isotropic response of an elastic–viscoplastic material that can be characterized by the symmetric tensor $\mathbf{B}_{\mathrm{e}}$. Using the work of Flory (1961), the tensor $\mathbf{B}_{\mathrm{e}}$ can be separated into a pure measure of elastic dilatation J_{e} and a pure measure of elastic distortional deformation $\mathbf{B}'_{\mathrm{e}}$ by the formulas

$$J_{\mathrm{e}} = \left[\det(\mathbf{B}_{\mathrm{e}})\right]^{1/2}, \quad \mathbf{B}'_{\mathrm{e}} = J_{\mathrm{e}}^{-2/3}\mathbf{B}_{\mathrm{e}}, \quad \det\left(\mathbf{B}'_{\mathrm{e}}\right) = 1. \tag{2.11}$$

Moreover, motivated by the developments in (Rubin and Chen, 1991; Rubin and Yarin, 1993; Rubin, 1994; Rubin and Attia, 1996), evolution equations can be specified for J_{e} and $\mathbf{B}'_{\mathrm{e}}$ in the forms

$$\dot{J}_{\mathbf{e}} = J_{\mathbf{e}}\left[\mathbf{D}\cdot\mathbf{I} - A_{\mathrm{p}}\right],$$

$$\dot{\mathbf{B}}'_{\mathrm{e}} = \mathbf{L}\mathbf{B}'_{\mathrm{e}} + \mathbf{B}'_{\mathrm{e}}\mathbf{L}^{\mathrm{T}} - \frac{2}{3}(\mathbf{D}\cdot\mathbf{I})\mathbf{B}'_{\mathrm{e}} - \mathbf{A}_{\mathrm{p}}, \tag{2.12}$$

where the scalar A_{p} and the symmetric tensor $\mathbf{A}_{\mathrm{p}}$ need to be specified by constitutive equations that characterize the relaxation effects of inelastic deformations (which can include both plasticity and microfracturing). Furthermore, since $\mathbf{B}'_{\mathrm{e}}$ is a unimodular tensor $(2.11)_3$ the quantity $\mathbf{A}_{\mathrm{p}}$ must satisfy the restriction that

$$\mathbf{A}_{\mathrm{p}}\cdot\mathbf{B}'^{-1}_{\mathrm{e}} = 0. \tag{2.13}$$

As a special case, $\mathbf{A}_{\mathrm{p}}$ can be taken in the form (Rubin and Attia, 1996)

$$\mathbf{A}_{\mathrm{p}} = \Gamma_{\mathrm{p}}\left[\mathbf{B}'_{\mathrm{e}} - \left\{\frac{3}{\mathbf{B}'^{-1}_{\mathrm{e}}\cdot\mathbf{I}}\right\}\mathbf{I}\right], \quad \Gamma_{\mathrm{p}} \geqslant 0, \tag{2.14}$$

where Γ_{p} is a non-negative function to be specified. This form for $\mathbf{A}_{\mathrm{p}}$ ensures that inelastic deformation causes $\mathbf{B}'_{\mathrm{e}}$ to tend to approach $\mathbf{I}$, which is consistent with elastic distortional strain approaching zero. Also, the evolution eqns (2.12) are integrated subject to initial conditions and it is assumed that $J_{\mathrm{e}} = 1$ and $\mathbf{B}'_{\mathrm{e}} = \mathbf{I}$ in the reference configuration. In addition, it is noted that if A_{p} and $\mathbf{A}_{\mathrm{p}}$ vanish then eqns (2.12) can be integrated to yield $J_{\mathrm{e}} = J = \det(\mathbf{F})$ and $\mathbf{B}_{\mathrm{e}} = \mathbf{B} = \mathbf{F}\mathbf{F}^{\mathrm{T}}$, with $\mathbf{F} = \partial\mathbf{x}/\partial\mathbf{X}$ being the

deformation gradient. Therefore, when inelastic effects vanish this theory can recover general nonlinear isotropic elastic response.

For a dry porous material it is common to separate an element of volume dV in the reference configuration into solid volume dV_s and pore volume dV_p and to separate an element of volume dv in the present configuration into solid volume dv_s and pore volume dv_p, such that

$$dV = dV_s + dV_p, \quad dv = dv_s + dv_p. \tag{2.15}$$

Also, the porosity Φ in the reference configuration and the porosity ϕ in the present configuration are defined by

$$\Phi = \frac{dV_p}{dV}, \quad \phi = \frac{dv_p}{dv}, \tag{2.16}$$

and the total relative volume J and the solid relative volume J_s are defined by

$$J = \frac{dv}{dV}, \quad J_s = \frac{dv_s}{dV_s}. \tag{2.17}$$

Next, assuming that changes in porosity are mainly due to inelastic deformations, the value of J_e is set equal to J_s so it can be expressed in the form

$$J_e = J_s = \frac{1-\phi}{1-\Phi}J. \tag{2.18}$$

Moreover, since J is determined by the evolution equation

$$\dot{J} = J(\mathbf{D}\cdot\mathbf{I}), \tag{2.19}$$

it follows that the inelastic deformation rate A_p in $(2.12)_1$ can be related to the change in porosity by the equation

$$A_p = \frac{\dot{\phi}}{1-\phi}. \tag{2.20}$$

For elastically isotropic response the Helmholtz free energy ψ can depend on the elastic deformation $\mathbf{B}_e$ only through its three invariants. These invariants include J_e and the two independent nontrivial invariants of the elastic distortional deformation $\mathbf{B}'_e$, which can be written as

$$\alpha_1 = \mathbf{B}'_e\cdot\mathbf{I}, \quad \alpha_2 = \mathbf{B}'_e\cdot\mathbf{B}'_e. \tag{2.21}$$

Here, for simplicity, the Helmholtz free energy is taken to be a function only of the variables

$$\{J_e, \alpha_1, \theta\}. \tag{2.22}$$

In particular, the Helmholtz free energy ψ_s of a nonporous solid is specified by

$$\rho_{s0}\psi_s = \rho_{s0}\hat{\psi}_{s1}(J_e,\theta) + \tfrac{1}{2}G(J_e,\theta)\,(\alpha_1 - 3), \tag{2.23}$$

where ρ_{s0} is the mass density of the nonporous solid in its reference configuration and G is a measure of its shear modulus that can be dependent on dilatation and temperature.

Letting ρ_0 be the mass density of the dry porous solid in its reference configuration it follows from (2.15) and (2.16) that

$$\rho_0 = (1-\Phi)\rho_{s0}. \tag{2.24}$$

Moreover, the conservation of mass of the porous material requires

$$\rho J = \rho_0, \tag{2.25}$$

so that with the help of (2.18), (2.24) and (2.25) it can be shown that

$$\rho = (1-\phi)\rho_s, \quad \rho_s J_e = \rho_{s0}, \quad \rho J_e = (1-\phi)\rho_{s0}, \tag{2.26}$$

where ρ_s is the current mass density of the solid. Now, for a dry porous media it is assumed that the Helmholtz free energy ψ is equal to that of the nonporous solid (see Rubin et al. 1996)

$$\psi = \psi_s, \tag{2.27}$$

and that η and $\mathbf{T}$ depend only on $\{\mathbf{B}_e, \theta\}$ while ξ' also depends on the rates $\{\dot{\phi}, \Gamma_p\}$. Thus, the balance of angular momentum (2.8) and the balance of energy (2.5) are satisfied by the specifications

$$\eta = \eta_s = \eta_{sl} + \eta_s', \quad \eta_{sl} = -\frac{\partial \hat{\psi}_{sl}}{\partial \theta}, \quad \rho_{s0}\eta_s' = -\frac{1}{2}\frac{\partial G}{\partial \theta}(\alpha_1 - 3),$$

$$\varepsilon = \psi + \theta\eta = \varepsilon_{sl} + \varepsilon_s', \quad \varepsilon_{sl} = \psi_{sl} + \theta\eta_{sl}, \quad \rho_{s0}\varepsilon_s' = \frac{1}{2}\left[G - \theta\frac{\partial G}{\partial \theta}\right](\alpha_1 - 3),$$

$$\mathbf{T} = -p\mathbf{I} + \mathbf{T}', \quad \mathbf{T}' \cdot \mathbf{I} = 0,$$

$$p = (1-\phi)p_s, \quad p_s = p_{sl} + p_s',$$

$$p_{sl} = -\rho_{s0}\frac{\partial \hat{\psi}_{sl}}{\partial J_e}, \quad p_s' = -\frac{1}{2}\frac{\partial G}{\partial J_e}(\alpha_1 - 3),$$

$$\mathbf{T}' = (1-\phi)\mathbf{T}_s', \quad \mathbf{T}_s' = J_e^{-1} G \mathbf{B}_e'',$$

$$\mathbf{B}_e'' = \left[\mathbf{B}_e' - \frac{1}{3}(\mathbf{B}_e' \cdot \mathbf{I})\mathbf{I}\right],$$

$$\xi' = \xi_\phi' + \xi_d', \quad \rho\theta\xi_\phi' = -p\left[\frac{\dot{\phi}}{1-\phi}\right],$$

$$\rho\theta\xi_d' = \frac{1}{2}(1-\phi)\Gamma_p J_e^{-1} G\left[\mathbf{B}_e' \cdot \mathbf{I} - \left\{\frac{9}{\mathbf{B}_e'^{-1} \cdot \mathbf{I}}\right\}\right], \tag{2.28}$$

where p is the pressure, $\mathbf{T}'$ is the deviatoric stress, $\mathbf{B}_e''$ is the deviatoric part of $\mathbf{B}_e'$, ξ_ϕ' is the specific internal rate of production of entropy due to porous compaction and dilation, and ξ_d' is the specific internal rate of production of entropy due to inelastic distortional deformation. In the above, $\eta_s, \varepsilon_s, p_s$ and $\mathbf{T}_s'$ are functional forms that characterize the response of the nonporous solid $[\Phi = \phi = 0, J_e = J]$,

and it is noted that the form $(2.28)_9$ is consistent with the model proposed by Carroll and Holt (1972). Moreover, for small elastic distortional deformations (Rubin and Attia, 1996) it can be shown that the rate of dissipation due to distortional deformation (2.28) can be approximated by the expression

$$\rho\theta\xi'_{\rm d} = \tfrac{1}{2}(1-\phi)\Gamma_{\rm p}J_{\rm e}^{-1}G\mathbf{B}''_{\rm e}\cdot\mathbf{B}''_{\rm e}, \tag{2.29}$$

which is automatically non-negative.

Many constitutive models for shock waves assume that the pressure $p_{\rm s}$ is determined by a Mie–Gruneisen equation of state. Following the work in Rubin (1987a) $p_{\rm sl}$ is related to $\varepsilon_{\rm sl}$ by a Mie–Gruneisen-type equation of the form

$$p_{\rm sl} = p_{\rm sH} + \rho_{\rm s}\gamma_{\rm s}[\varepsilon_{\rm sl} - \varepsilon_{\rm sH}], \quad e_{\rm v} = 1 - J_{\rm e},$$

$$p_{\rm sH} = \rho_{\rm s0}D^2 e_{\rm v}, \quad \varepsilon_{\rm sH} = \frac{p_{\rm sH}e_{\rm v}}{2\rho_{\rm s0}}, \tag{2.30}$$

where $p_{\rm sH}$ and $\varepsilon_{\rm sH}$ are the pressure and internal energy associated with the Hugoniot of the solid material, $\gamma_{\rm s}$ is the Gruneisen gamma which controls the temperature dependence of the pressure, $e_{\rm v}$ is a measure of elastic volumetric compression and D is the shock velocity. Specifically, the model used by Steinberg (1991), suggests that

$$\gamma_{\rm s} = \gamma_{\rm s0}J_{\rm e} + b_{\rm s}e_{\rm v},$$

$$D = \frac{C_{\rm s0}}{1 - S_1 e_{\rm v} - S_2 e_{\rm v}^2 - S_3 e_{\rm v}^3}, \quad \text{for } J_{\rm e} \leqslant 1,$$

$$D^2 = \frac{C_{\rm s0}^2}{J_{\rm e}\left[1 - (\gamma_{\rm s0}/2)e_{\rm v}\right]}, \quad b_{\rm s} = 0, \quad \text{for } J_{\rm e} > 1, \tag{2.31}$$

where $\gamma_{\rm s0}$, $b_{\rm s}$, $C_{\rm s0}$, S_1, S_2, S_3 are material constants. Moreover, using (Rubin, 1987a) it can be shown that the functions

$$\begin{aligned}
\rho_{\rm s0}\psi_{\rm s1} &= \rho_{\rm s0}c_{\rm sv}\left[(\theta-\theta_0) - \theta\ln\ (\theta/\theta_0)\right] - (\theta-\theta_0)f_1(J_{\rm e}) + f_2(J_{\rm e}) \\
p_{\rm s1} &= -\rho_{\rm s0}\frac{\partial\psi_{\rm s1}}{\partial J_{\rm e}} = (\theta-\theta_0)\frac{{\rm d}f_1}{{\rm d}J_{\rm e}} - \frac{{\rm d}f_2}{{\rm d}J_{\rm e}}, \\
\rho_{\rm s0}\eta_{\rm s1} &= -\rho_{\rm s0}\frac{\partial\psi_{\rm s1}}{\partial\theta} = \rho_{\rm s0}c_{\rm sv}\ln(\theta/\theta_0) + f_1 \\
\rho_{\rm s0}\varepsilon_{\rm s1} &= \rho_{\rm s0}c_{\rm sv}(\theta-\theta_0) + \theta_0 f_1 + f_2,
\end{aligned} \tag{2.32}$$

are consistent with the constitutive eqns (2.28) and the Mie–Gruneisen form (2.30) provided that f_1 and f_2 satisfy the differential equations

$$\frac{{\rm d}f_1}{{\rm d}J_{\rm e}} = \frac{\rho_{\rm s0}c_{\rm sv}\gamma_{\rm s}}{J_{\rm e}}, \quad f_1(1) = 0,$$

$$\frac{{\rm d}f_2}{{\rm d}J_{\rm e}} + \left[\frac{\gamma_{\rm s}}{J_{\rm e}}\right]f_2 = -\frac{\gamma_{\rm s}\theta_0 f_1}{J_{\rm e}} + \frac{\rho_{\rm s0}\gamma_{\rm s}\varepsilon_{\rm sH}}{J_{\rm e}} - p_{\rm sH}, \quad f_2(1) = 0. \tag{2.33}$$

In these equations θ_0 is the reference value of temperature and c_{sv} is the constant specific heat at constant volume. For the special form (2.31) of the Gruneisen gamma the function f_1 is given by

$$f_1 = \rho_{s0} c_{sv}\big[b_s \ln\ (J_e) - \big(\gamma_{s0} - b_s\big)e_v\big], \tag{2.34}$$

and f_2 can be obtained by quadratures.

Also, the functional form of the shear modulus $G(J_e, \theta)$ can be specified (Rubin, 1987a) to include dependence on pressure p_{s1} and temperature in the form suggested by Steinberg et al. (1980). For example, G could be specified by the form

$$G(J_e, \theta) = G_0\big[1 + A_1 J_e^{1/3} p_{s1} + A_2(\theta - \theta_0)\big], \tag{2.35}$$

where G_0, A_1, A_2 are material constants.

With regard to the second law of thermodynamics it can be shown by expressing $\mathbf{B}'_e$ in its spectral form in terms of its eigenvalues and eigenvectors that inelastic distortional deformation is dissipative

$$\rho\theta\xi'_d \geqslant 0, \tag{2.36}$$

even for large inelastic deformations so that (2.10) places a restriction on the rate of change of porosity

$$-p\left[\frac{\dot{\phi}}{1-\phi}\right] + \rho\theta\xi'_d \geqslant 0. \tag{2.37}$$

Also, for the usual form of Fourier heat conduction the entropy flux $\mathbf{p}$ is given by

$$\mathbf{p} = -\frac{k}{\theta}\mathbf{g}, \tag{2.38}$$

so that (2.9) requires the heat conduction coefficient k to be positive.

3. Evolution of plastic distortional deformation

The evolution equation for elastic distortional deformation characterized by $(2.12)_2$ and (2.14) requires the specification of a functional form for Γ_p. For metal plasticity it is common to define the von Mises effective stress σ_e by the formula

$$\sigma_e^2 = \frac{3}{2}\mathbf{T}' \cdot \mathbf{T}', \tag{3.1}$$

and to assume that plasticity limits the magnitude of σ_e. In particular, for rate-independent plasticity a yield function is introduced of the form

$$g = \frac{\sigma_e - Y}{Y_0} \leqslant 0, \tag{3.2}$$

where Y is a function that determines the yield strength in uniaxial stress conditions and Y_0 is the value of Y in the reference configuration. Elastic response corresponds to $g < 0$ and $g = 0$ determines the elastic–plastic boundary. For elastic response the value of Γ_p vanishes whereas for plastic response the value of Γ_p is determined by a consistency condition (e.g. Rubin and Attia, 1996) that requires $\dot{g}$ to vanish during loading.

For viscoplastic response the quantity Γ_p in (2.12) is taken to be a function of the von Mises effective stress σ_e and the yield strength Y. For example, within the context of a unified viscoplastic theory without a yield surface, Γ_p could be specified by the functional form proposed in (Bodner and Partom, 1972; Bodner, 1987) or by a modified form proposed in (Rubin, 1987b).

In general, the numerical methods developed in (Rubin, 1989; Rubin and Attia, 1996) show that integration of the evolution equation for determining elastic distortional deformation reduces to the determination of the zero of a single scalar equation. Usually, iterative methods are required to solve this equation. However, for the simple overstress model proposed by Swegle and Grady (1985, 1986) Γ_p is specified in terms of a material constant Γ_{p0} by the form

$$\Gamma_p = \Gamma_{p0}\left[\frac{3G}{\sigma_e}\right]\left[\frac{\langle \sigma_e - Y\rangle}{Y_0}\right]^2, \tag{3.3}$$

and this scalar equation can be solved analytically (Rubin, 1990). Moreover, in (3.3) and throughout the text it is convenient to use the Heaviside function $H(x)$ and the McAuley brackets $\langle x\rangle$ which are defined by

$$H(x) = \begin{cases} 0 & \text{for } x \leqslant 0 \\ 1 & \text{for } x > 0 \end{cases},$$

$$\langle x\rangle = \begin{cases} 0 & \text{for } x < 0 \\ x & \text{for } x \geqslant 0 \end{cases}. \tag{3.4}$$

The yield strength for metals is also dependent on a hardening variable which for a simplified model can be related directly to the equivalent plastic strain ε_p that has accumulated from an annealed state. In (Rubin and Attia, 1996) it was shown that for small elastic distortional deformations the inelastic distortional deformation rate associated with $(2.12)_1$ can be approximated by

$$\mathbf{D}_p = \tfrac{1}{2}\Gamma_p \mathbf{A}_p \approx \tfrac{1}{2}\Gamma_p \mathbf{B}_e'', \tag{3.5}$$

so the equivalent plastic strain is determined by the evolution equation

$$\dot{\varepsilon}_p = \left[\tfrac{2}{3}\mathbf{D}_p \cdot \mathbf{D}_p\right]^{1/2}, \tag{3.6}$$

which is integrated subjected to the condition that ε_p vanishes in the reference configuration.

Since the model developed here is intended to apply to both metals and geological porous materials, it is necessary to introduce a number of additional physical phenomena that influence the yield strength Y. This is done by assuming a simple multiplicative form with Y being given by

$$Y = Y_0 F_1(\varepsilon_p) F_2(p) F_3(\Omega) F_4(\beta, p) F_5(J_e, \theta) F_6(\phi) F_7(\omega, p). \tag{3.7}$$

The function F_1 is used to model the effects of hardening exhibited by metals and is taken in the form

$$F_1(\varepsilon_p) = k_1 + (1 - k_1)\exp\left(-k_2\varepsilon_p\right), \quad k_1 \geqslant 1, \tag{3.8}$$

where k_1 and k_2 are positive material constants. The value of k_1 determines the maximum increase in yield strength due to hardening and the value of k_2 determines how rapidly F_1 attains this maximum value.

The function F_2 is used to model the pressure sensitivity of rocks and is taken in the form

$$F_2(p) = 1 + \frac{k_3\langle p\rangle}{1 + k_4\langle p\rangle}, \tag{3.9}$$

where k_3 and k_4 are additional non-negative material constants. If k_4 is positive then F_2 will increase to a maximum value of $(1 + k_3/k_4)$, otherwise, F_2 will increase linearly with pressure. Also, the value of k_3 determines how rapidly F_2 increases.

The function F_3 is used to model the decrease in yield strength of rocks due to distortional deformation damage and is taken in the form

$$F_3(\Omega) = f(\Omega, k_5, k_6), \quad 0 \leqslant k_5 \leqslant 1, \quad k_6 > 0, \tag{3.10}$$

where k_5 and k_6 are material constants and the function $f(\Omega, k_5, k_6)$ is specified by

$$f(\Omega, k_5, k_6) = 1 - k_5 \exp\left[-\frac{k_6(1-\Omega)^2}{\Omega}\right],$$

$$f(0, k_5, k_6) = 1, \quad f(1, k_5, k_6) = 1 - k_5 \geqslant 0,$$

$$\frac{\partial f}{\partial \Omega}(0, k_5, k_6) = 0, \quad \frac{\partial f}{\partial \Omega}(1, k_5, k_6) = 0. \tag{3.11}$$

This function is introduced to smooth out the transition at the onset of damage. In particular, it can be shown that $f(\Omega, k_5, k_6)$ has a zero slope at $\Omega = 0$ and $\Omega = 1$ and that onset of damage becomes more rapid as the value of k_6 is decreased. For simplicity, the measure of damage Ω due to distortional deformation is determined by the formula

$$\Omega = \mathrm{Min}\left[\frac{\varepsilon_p}{\varepsilon_d}, 1\right], \tag{3.12}$$

where the material constant ε_d determines the value of equivalent plastic strain at which complete damage has occurred ($\Omega = 1$ and $F_3 = 1 - k_5$).

Often geological materials and concrete simulants exhibit a lower value of strength in tension than in compression. To model this effect the yield strength Y is assumed to depend on the Lode angle β which determines the state of deviatoric stress. Specifically, the function, F_4 is defined by (Rubin and Attia, 1990; Rubin, 1991)

$$\sin(3\beta) = -\frac{27\det(\mathbf{T}')}{2\sigma_e^3}, \quad -\frac{\pi}{6} \leqslant \beta \leqslant \frac{\pi}{6},$$

$$a_0 = 2Q_1^2(Q_2 - 1), \quad a_1 = \sqrt{3}Q_2 + 2Q_1(Q_2 - 1), \quad a_2 = Q_2,$$

$$a = \frac{-a_1 + \sqrt{a_1^2 - 4a_2a_0}}{2a_2}, \quad b = (2Q_1 + a)^2 - 3,$$

$$b_0 = -\frac{1}{4}\left(3 + b - a^2\right), \quad b_1 = a\left[\cos(\beta) - a\sin(\beta)\right],$$

$$b_2 = \left[\cos(\beta) - a\sin(\beta)\right]^2 + b\sin^2(\beta),$$

$$F_4(\beta, p) = \frac{-b_1 + \sqrt{b_1^2 - 4b_2 b_0}}{2b_2}. \tag{3.13}$$

In these formulas $Q_1(p)$ and $Q_2(p)$ are functions of pressure p which can be related to the strength for stress states of pure torsion (TOR) and triaxial extension (TXE) (which includes uniaxial tension). In particular, it can be shown that

$$F_4 = 1 \quad \text{for TXC with } \beta = \frac{\pi}{6},$$

$$F_4 = Q_1 \quad \text{for TOR with } \beta = 0,$$

$$F_4 = Q_2 \quad \text{for TXE with } \beta = -\frac{\pi}{6}. \tag{3.14}$$

For the simple case of a von Mises yield surface the values of Q_1 and Q_2 are equal to unity

$$Q_1 = Q_2 = 1 \quad \text{for von Mises,} \tag{3.15}$$

whereas for a Mohr–Coulomb type yield surface the value of Q_1 is related to Q_2 by the formula

$$Q_1 = \frac{\sqrt{3}Q_2}{1 + Q_2}. \tag{3.16}$$

Moreover, for the Tresca condition, Q_2 equals unity with Q_1 being given by (3.16).

To motivate an expression for Q_2 it is of interest to consider the case of uniaxial stress in tension (TXE) from the reference configuration ($\varepsilon_p = \Omega = 0$) for which

$$\sigma_e = Y = Q_2 Y_0, \quad p = -\frac{Y}{3}. \tag{3.17}$$

Now, it is assumed that tensile failure initiates and porosity tends to increase when the pressure attains the negative value ($-p_d$). Thus, since (3.17) indicates that both the pressure and the yield strength remain proportional to each other in uniaxial stress, it is reasonable to specify Q_2 by the form

$$Q_2 = \frac{3p_d}{Y_0}. \tag{3.18}$$

This form allows the value of p_d to be directly related to experimental data for failure in uniaxial tension.

For relatively low pressure it is reasonable to consider a Mohr–Coulomb type yield surface with Q_1 specified by (3.16). However, for high pressures it is expected that a Mises type yield surface is more appropriate. Therefore, the functions Q_1 and Q_2 are specified to be pressure dependent by the forms

$$
\begin{aligned}
Q_1 &= 1 + (Q_{10} - 1)Q(p), \quad Q_{10} = \frac{\sqrt{3}Q_{20}}{1 + Q_{20}}, \\
Q_2 &= 1 + (Q_{20} - 1)Q(p), \quad Q_{20} = \frac{3p_{\mathrm{d}}}{Y_0}, \\
Q(p) &= \exp\left(-q\langle 3p/Y_0 - 1\rangle\right), \quad Q \geqslant 0,
\end{aligned}
\tag{3.19}
$$

where q is a material constant. These functions model a smooth transition from Mohr–Coulomb behavior for $p \leqslant Y_0/3$ to Mises behavior for $p \gg Y_0/3$ (and $q > 0$).

The function $F_5(J_e, \theta)$ in (3.7) can be specified in a form similar to that proposed by Steinberg et al. (1980) (with p replaced by p_{s1} here) to model the pressure and temperature dependence of the yield strength exhibited by metals. For example, the function F_5 could be specified by

$$
F_5(J_e, \theta) = \frac{G(J_e, \theta)}{G_0},
\tag{3.20}
$$

where the shear modulus G was defined in (2.35).

The function $F_6(\phi)$ in (3.7) is specified by

$$
F_6(\phi) = \frac{1 - \phi}{1 - \Phi},
\tag{3.21}
$$

which incorporates the feature of the Gurson model (Gurson, 1977) that the yield strength for zero pressure vanishes as the porosity approaches unity. Also, the function F_7 models the effect of damage due to porous compaction and dilation and it is specified by

$$
\begin{aligned}
&F_7 = 1 \quad \text{for } p > -p_{\mathrm{d}}, \\
&F_7 = f(\omega, k_7, k_8) \quad \text{for } p \leqslant -p_{\mathrm{d}}, \quad 0 \leqslant k_7 < 1, \quad k_8 > 0,
\end{aligned}
\tag{3.22}
$$

where $f(\omega, k_7, k_8)$ is the function defined by (3.11), with k_7 and k_8 being material constants, p_{d} being a function to be specified later, and ω being a measure of damage due to porosity changes which is also specified later.

The analytical functional forms for F_1–F_7 in (3.7) have been specified to provide reasonable response for many materials. However, it is also possible to specify these functions in tabular form for more flexibility in accurately modeling specific experimental data.

4. Evolution of porosity

In general, the second law of thermodynamics (2.37) places restrictions on the evolution equation for porosity and plasticity. Often the first term in (2.37) is non-negative with porous compaction ($\dot{\phi} < 0$) occurring for positive pressure and porous dilation ($\dot{\phi} > 0$) occurring for negative pressure. However, experiments on glass (Glenn et al., 1990) indicate that dynamic loading can cause microfracturing that tends to increase the porosity of the damaged glass even when the pressure has remained positive. The constitutive equations discussed in this section attempt to model all of these situations.

In order to propose constitutive equations for the evolution of porosity it is convenient to define the minimum value $\phi_{\min}$ and maximum value $\phi_{\max}$ of ϕ for all time

$$
\phi_{\min} = \mathrm{Min}\left[\phi\right], \quad \phi_{\max} = \mathrm{Max}\left[\phi\right].
\tag{4.1}
$$

Now, consider the case of a brittle material-like glass which initially has zero porosity. Such a material can break under tension creating significant local porosity. However, it can also be damaged by distortional deformation under compression or tension causing cloudiness due to creation of porosity at fractured surfaces. Here, it is assumed that when the material is damaged by distortional deformation the porosity tends to increase to the value ϕ^*. This response is modeled by the constitutive equation

$$\dot{\phi} = (1-\phi)\left[\frac{m_d(\rho\theta\xi_d')}{\text{Max}\,(p,p^*)}\right]H(\phi^*-\phi) \geqslant 0, \quad \text{for } \phi_{max} < \phi^* \quad \text{and} \quad p > -p_d. \tag{4.2}$$

where m_d, ϕ^* and p^* are material constants, p_d is a positive function to be specified, and the term Max (p, p^*) is introduced instead of the pressure p to eliminate the singularity that would occur at zero pressure. The Heaviside function in (4.2) causes the porosity to remain less than ϕ^*, which is a measure of the misfit of fractured pieces of material under compression. Moreover, the functional form was chosen so that the second law of thermodynamics (2.37) will be satisfied provided that

$$(\rho\theta\xi_d')\left[1-\frac{m_d p}{\text{Max}\,(p,p^*)}\right] \geqslant 0, \quad 0 \leqslant m_d \leqslant 1, \tag{4.3}$$

with the maximum porous dilation occurring when m_d equals unity. Also, it follows that if ϕ^* vanishes then porous dilatation due to distortional deformation is not possible.

Models for dynamic failure of solids have been reviewed by Curran et al. (1987). For elastic–perfectly plastic metals the Gurson model (Gurson, 1977) has been used to determine nucleation, growth and compaction of voids. A generalization of this model (Johnson and Addessio, 1988) has also been used to model the spallation process in dynamic impact experiments. For porous geological materials, porous compaction and dilation is usually caused by creation, opening and closing of microfractures. Although these mechanisms are different from those that occur in metals, both materials are modeled here using the same equations.

The Gurson model (Gurson, 1977) introduces an algebraic equation of stress and porosity which serves as a yield function that must be solved either in rate form or iteratively to determine the material response. Since the dependence of the pressure on porosity can be quite nonlinear, the solution of equations of this type can pose numerical difficulties. In order to eliminate many of these numerical difficulties, the constitutive equations for porosity proposed here are formulated as rate-dependent evolution equations like (4.2).

Specifically, additional evolution equations for porous compaction are given by

$$\dot{\phi} = 0 \quad \text{for } \phi_{max} \geqslant \phi^* \quad \text{and} \quad -p_d \leqslant p \leqslant 0,$$

$$\dot{\phi} = -(1-\phi)\langle -\mathbf{D}\cdot\mathbf{I}\rangle H(\phi-\phi^*_{min}) \leqslant 0 \quad \text{for } \phi_{max} \geqslant \phi^* \quad \text{and} \quad 0 \leqslant p \leqslant p_c,$$

$$\dot{\phi} = -\Gamma_c\langle\phi-\phi^*_c\rangle \leqslant 0 \quad \text{for } \phi_{max} \geqslant \phi^* \quad \text{and} \quad p > p_c, \tag{4.4}$$

and the evolution equation for porous dilation when the pressure is more negative than $(-p_d)$ is given by

$$\dot{\phi} = \Gamma_d\left[1+\left(\frac{\phi^*_d}{\phi_s}\right)^m\right]\left[\frac{\langle\phi^*_d-\phi\rangle}{\phi_s}\right]^n \geqslant 0 \quad \text{for } p \leqslant -p_d. \tag{4.5}$$

Table 1
Summary of the equations for porous compaction and dilation

Range of pressure	Range of ϕ_{max}	Equation	Type of deformation
$p \leqslant -p_d$	Any value	(4.5)	Porous dilation
$-p_d < p < 0$	$\phi_{max} < \phi^*$	(4.2)	Porous dilation
	$\phi^* \leqslant \phi_{max}$	$(4.4)_1$	Constant porosity
$0 \leqslant p \leqslant p_c$	$\phi_{max} < \phi^*$	(4.2)	Porous dilation
	$\phi^* \leqslant \phi_{max}$	$(4.4)_2$	Porous compaction
$p_c < p$	$\phi_{max} < \phi^*$	(4.2)	Porous dilation
	$\phi^* \leqslant \phi_{max}$	$(4.4)_3$	Porous compaction

In addition, a measure of damage ω due to porous compaction and dilation is defined by the evolution equation

$$\dot{\omega} = \frac{1}{\varepsilon_v}\frac{|\dot{\phi}|}{(1-\phi)}H(1-\omega), \tag{4.6}$$

which is integrated subject to the condition that ω vanishes in the reference configuration. Also, the Heaviside function ensures that ω never is greater than unity.

The evolution eqns (4.2), (4.4)–(4.6) introduce ten non-negative constants $\{m_d, \phi^*, p^*, \Gamma_c, p_c, \Gamma_d, \phi_s, m, n, \varepsilon_v\}$ and four functions $\{\phi_c^*, \phi_{min}^*, \phi_d^*, p_d\}$. For convenience the range of applicability of these equations are summarized in Table 1. An important feature of eqns (4.2), (4.4) and (4.5) is that they tend to cause the porosity ϕ to approach values determined by specified functions (e.g. ϕ^*, ϕ_c^*, ϕ_{min}^*, ϕ_d^*). Also, the rate at which ϕ approaches these values is determined by $(m_d, \Gamma_c, \Gamma_d)$. Thus, the main features of the material response can be ensured by proper choice of the constant ϕ^* and the functions $(\phi_c^*, \phi_{min}^*, \phi_d^*)$.

For example, when eqn $(4.4)_3$ is active the porosity tends to decrease to the value ϕ_c^*. Consequently, the function ϕ_c^* can be tabulated to match experimental data for compaction. Alternatively, it is possible to specify the function by an approximate analytical form.

In order to propose analytical forms for some of these functions it is noted that the magnitude of the pressure at the onset of compaction and during expansion is rather low. Specifically, for hydrostatic $(\alpha_1 = 3)$ expansion $(J_e > 1)$ eqns $(2.28)_{9,10}$, (2.30) and (2.31) yield

$$p = (1-\phi)\left[\rho_{s0}C_{s0}^2\left(\frac{1}{J_e}-1\right) + \rho_{s0}\gamma_{s0}\varepsilon_{s1}\right]. \tag{4.7}$$

Moreover, to motivate some of the functional forms this expression for pressure is assumed to hold also for small values of compression $(e_v \ll 1)$. During compaction from the reference state (with no macroscopic distortional deformation, $\rho\theta\xi_d' = 0$), the porosity remains constant $(\phi = \Phi)$ until the pressure reaches the crush pressure p_c. This means that $J_e = J$ and the value J_c of J associated with the onset of compaction is obtained by solving (4.7) to deduce that

$$\frac{1}{J_c} = 1 + \frac{p_c}{(1-\Phi)\rho_{s0}C_{s0}^2}, \tag{4.8}$$

where thermal effects have been neglected $(\gamma_{s0} = 0)$. Moreover, if further compression were to keep the pressure p in (4.7) equal to the constant value p_c, then ϕ would be determined by the expression

$$\phi = \Phi - (1-\Phi)\left[\frac{1}{J} - \frac{1}{J_c}\right], \quad \text{for } p = p_c. \tag{4.9}$$

However, the pressure typically increases during compaction. Also, it is of interest to include the effect of shear enhanced compaction that is exhibited by cap models of the type reviewed in (Chen and Baladi, 1985).

To this end, consider the function ϕ_c^{**} defined by

$$\phi_c^{**} = \Phi - c_1(1-\Phi)\left[\frac{1}{J} - \frac{1}{J_c}\right]F_8 \quad \text{for } \frac{1}{J_c} \leqslant \frac{1}{J} \leqslant c_2,$$

$$\phi_c^{**} = \phi_2 \exp\left[-\frac{c_1(1-\Phi)F_8}{\phi_2}\left\langle\frac{1}{J} - c_2\right\rangle\right] \quad \text{for } c_2 < \frac{1}{J},$$

$$\phi_2 = \Phi - c_1(1-\Phi)\left[c_2 - \frac{1}{J_c}\right]F_8,$$

$$F_8(\sigma_e, Y) = \left[1 + c_3\left(\frac{1}{c_1} - 1\right)\right] - c_3\left(\frac{1}{c_1} - 1\right)\left[\text{Max}\left\{0, 1 - (\sigma_e/Y)^2\right\}\right]^{c_4},$$

$$0 \leqslant c_1 \leqslant 1, \quad \frac{1}{J_c} \leqslant c_2 \leqslant \frac{1}{J_c} + \frac{\Phi}{c_1(1-\Phi)F_8},$$

$$0 \leqslant c_3 \leqslant 1, \quad c_4 \geqslant 0 \tag{4.10}$$

where the functions ϕ_c^{**} are chosen to be continuous and have continuous first derivatives at the transition points. The material constants c_1 and c_2 control the shape of the pressure curve during compaction and the function F_8 controls shear enhanced compaction with the material constants $\{c_3, c_4\}$. The functional form (4.10) for $1/J \leqslant c_2$ is similar to (4.9) with porosity being a linear function of $1/J$. Therefore, for $c_1 = 0$ the material response is stiff with porosity remaining constant, whereas for $c_1 = 1$ the material response is soft with pressure remaining nearly constant as porosity decreases. In particular, it can be shown by replacing ϕ in (4.7) by ϕ_c^{**} and ignoring energy effects ($\gamma_{s0} = 0$) and shear enhanced compaction ($F_8 = 1$) that at the onset of compaction ($J = J_c$)

$$\frac{dp}{dJ} = -\frac{\rho_{s0}C_{s0}^2(1-\Phi)(1-c_1)}{J_c^2}, \quad \text{for } J = J_c, \phi = \phi_c^{**}, \quad F_8 = 1. \tag{4.11}$$

Thus, it follows that the slope of the pressure during compaction will vanish when c_1 equals unity. Moreover, for $c_1 < 1$ and $c_3 > 0$, the value of ϕ_c^{**} decreases as deviatoric stress σ_e increases. For $c_4 > 0$ the derivative of F_8 with respect to σ_e vanishes when σ_e vanishes, which is consistent with a spherical cap model (Chen and Baladi, 1985). Also, since F_8 is taken to be a function of σ_e/Y it automatically incorporates the effects of hardening, pressure sensitivity, damage, Lode angle and porosity on shear enhanced compaction [see (3.7)].

Next, the functions ϕ_c^* and ϕ_{min}^* are defined by the expressions

$$\phi_c^* = \text{Max}\left[\phi_c^{**}, \phi^*\right], \quad \phi_{min}^* = \text{Max}\left[\phi_{min}, \phi^*\right] \quad \text{for } \phi_{max} \geqslant \phi^*. \tag{4.12}$$

Using these functions the evolution eqns (4.2), (4.4) and (4.5) predict the following features: for

$\phi_{\max} < \phi^*$ porous dilation can occur due to distortional deformation when the pressure is greater than $(-p_d)$ but porous compaction cannot occur; for $\phi_{\max} \geqslant \phi^*$ porous compaction can occur when the pressure is non-negative; and porous dilation can occur directly due to tensile failure when the pressure is less than $(-p_d)$ for any value of $\phi_{\max}$. Moreover, whenever the value of porosity ϕ becomes greater than ϕ^* then porous dilation due to distortional deformation ceases and porous compaction can only reduce the porosity back to the value ϕ^*, which is the minimum value for a fully fractured material.

The eqn $(4.4)_2$ is used to simulate fracture closure with negligible increase in pressure. In particular, if the material has been expanded, with ϕ greater than $\phi^*_{\min}$, and if the material is being compressed $(\mathbf{D} \cdot \mathbf{I} < 0)$, then when the pressure becomes non-negative compaction $(\dot{\phi} < 0)$ will occur with

$$\dot{\phi} = (1 - \phi)(\mathbf{D} \cdot \mathbf{I}). \tag{4.13}$$

Moreover, it can be seen from $(2.12)_1$ and (2.20) that (4.13) causes J_e to remain constant. This means that fractures that have been opened $(\phi > \phi^*_{\min})$ will tend to close with negligible pressure until ϕ attains the minimum value $\phi^*_{\min}$. Also, eqn $(4.4)_1$ indicates elastic response in tension $(p < 0)$ until the pressure becomes more negative than a dilation value $(-p_d)$.

Eqn (4.5) indicates that dilation $(\dot{\phi} > 0)$ will occur with the porosity ϕ increasing to the value ϕ^*_d when the pressure is less than the value $(-p_d)$. It is expected that the value of p_d will decrease towards zero as damage evolves. However, the value of p_d is required to remain positive. Thus, for example, p_d can be taken to have the simple form

$$p_d = p_{d0} f(\omega, k_7, k_8), \tag{4.14}$$

where p_{d0} is a material constant and the function $f(\omega, k_7, k_8)$ is specified (3.11). This causes the magnitude of the pressure and the yield strength to be reduced by the same factor. Also, it is expected that k_7 will have a value very close to unity in order to simulate near complete loss of strength in tension for both pressure and yield strength.

In order to motivate a functional form for ϕ^*_d it is noted that during porous dilation with negative pressure (4.5) the material tends to expand $(J_e > 1)$ so that in the absence of distortion $(\alpha_1 = 3)$ the pressure is given by the expression (4.7). Thus, a functional form for ϕ^*_d can be specified by setting $p = -p_d$ and $\phi = \phi^*_d$ in (4.7) and solving the equation for ϕ^*_d to obtain

$$\phi^*_d = 1 - \frac{\dfrac{1 - \Phi}{J} + \dfrac{p_d}{\rho_{s0} C^2_{s0}}}{1 - \dfrac{\gamma_{s0} e_{s1}}{C^2_{s0}}} \tag{4.15}$$

Note that for a constant value of J, the value of ϕ^*_d decreases and the value of J_e increases as the energy increases due to heating associated with material dissipation.

5. Numerical approximations

In standard wave propagation computer codes the equations of motion and the energy equation are integrated to determine the deformation and internal energy of each element. Then, the constitutive equations are integrated in each element over the time step to determine the stress field that is used to specify the equations of motion for the next time step. Also, if the constitutive equations are hyperelastic, like the ones proposed here, then the constitutive equation for internal energy (2.28) can be solved for the temperature.

In shock wave applications the value of pressure usually dominates that of the deviatoric stress. Therefore, the detailed model described by (2.30)–(2.35) is used to model full thermomechanical coupling in the constitutive equation for pressure. Here, attention is focused on robust numerical integration of the evolution equations for porosity and elastic distortional deformations. For simplicity, the common assumption is used that the equations for porosity can be integrated using estimates of the elastic distortional deformation. Then, the equations for elastic distortional deformation can be integrated using the predicted value of porosity. Also, attention will be focused on the case of dynamic loading which is adiabatic so that the effect of heat conduction is neglected [$k = 0$ in (2.38)].

At the beginning $t = t_1$ of a typical time step (t_1, t_2) the values of all relevant quantities are known. The numerical scheme estimates the value of all quantities at the end of the time step $t = t_2$ by assuming that the velocity gradient $\mathbf{L}$ is constant over the time interval. For convenience, the values of the quantities $\{J, \theta, \phi, \phi_{\max}, \phi^*_{\min}, p, p_{\rm d}, \sigma_{\rm e}, Y, \omega, \mathbf{B}'_{\rm e}, \mathbf{g}'_{\rm e}, \varepsilon_{\rm p}, \rho\theta\xi'_{\rm d}\}$ at beginning $(t = t_1)$ of the time step are denoted by

$$\left\{J_1, \theta_1, \phi_1, \phi_{\max 1}, \phi^*_{\min 1}, p_1, p_{\rm d1}, \sigma_{\rm e1}, Y_1, \omega_1, \mathbf{B}'_{\rm e1}, \mathbf{g}'_{\rm e1}, \varepsilon_{\rm p1}, \rho\theta\xi'_{\rm d1}\right\} \quad \text{at } t = t_1, \tag{5.1}$$

and the values of the same quantities at the end $(t = t_2)$ of the time step are denoted by

$$\left\{J_2, \theta_2, \phi_2, \phi_{\max 2}, \phi^*_{\min 2}, p_2, p_{\rm d2}, \sigma_{\rm e2}, Y_2, \omega_2, \mathbf{B}'_{\rm e2}, \mathbf{g}'_{\rm e2}, \varepsilon_{\rm p2}, \rho\theta\xi'_{\rm d2}\right\} \quad \text{at } t = t_2. \tag{5.2}$$

Also, the time interval is denoted by

$$\Delta t = t_2 - t_1. \tag{5.3}$$

Since the velocity gradient $\mathbf{L}$ is assumed to be constant over the time step the evolution eqn (2.19) yields

$$J_2 = J_1 \exp\left(\Delta t \mathbf{D} \cdot \mathbf{I}\right). \tag{5.4}$$

Next, values of the quantities $\{\phi^{**}_{\rm c}, \phi^{*}_{\rm c}, \phi^{*}_{\rm d}\}$ are determined using the functions (4.10), $(4.12)_1$, (4.15), the new value J_2 and the old values of all other independent variables

$$\phi^{**}_{\rm c}(J_2, \sigma_{\rm e1}, Y_1), \quad \phi^{*}_{\rm c}(J_2, \sigma_{\rm e1}, Y_1), \quad \phi^{*}_{\rm d}(J_2, \theta_1, p_{\rm d1}). \tag{5.5}$$

Thus, with the help of (5.5) and the old values (5.1) it can be determined which one of the evolution eqns (4.2), (4.4) or (4.5) is relevant. (In this regard, it should be mentioned that the critical value of pressure used to distinguish between these evolution equations was modified by subtracting a small value from $p_{\rm d}$ in order to eliminate numerical oscillations that occurred for small values of p_d.) If the relevant one of these equations predicts zero change in porosity then ϕ_2 is set equal to ϕ_1. Otherwise, one of these evolution equations will be relevant and predict nonzero change in porosity. Thus, when ϕ does not remain constant then the value of ϕ_2 is determined by one of the following expressions

$$\phi_2 = \text{Min}\left[1 - \left(1 - \phi_1\right)\exp\left\{-\Delta t\left[\frac{m_{\rm d}\left(\rho\theta\xi'_{\rm d1}\right)}{\text{Max}\left(p_1, p^*\right)}\right]\right\}, \phi^*\right] \quad \text{for (4.2)},$$

$$\phi_2 = \text{Max}\left[1 - \left(1 - \phi_1\right)\frac{J_1}{J_2}, \phi^*_{\min 1}\right] \quad \text{for } (4.4)_2,$$

$$\phi_2 = \phi^*_{\rm c} + \left(\phi_1 - \phi^*_{\rm c}\right)\exp\left\{-\Delta t\Gamma_{\rm c}\right\} \quad \text{for } (4.4)_3,$$

$$\phi_2 = \phi_d^* - \left[\text{Max}\left\{0, \left(\phi_d^* - \phi_1\right)^{(1-n)} - (1-n)\Gamma_d \Delta t\left\{1 + \left(\phi_d^*/\phi_s\right)^m\right\}/\phi_s^n\right\}\right]^{1/(1-n)}$$

for (4.5) with $n < 1$,

$$\phi_2 = \phi_d^* - \left(\phi_d^* - \phi_1\right)\exp\left[-\Gamma_d \Delta t\left\{1 + \left(\phi_d^*/\phi_s\right)^m\right\}/\phi_s\right] \quad \text{for (4.5) with } n = 1,$$

$$\phi_2 = \phi_d^* - \frac{\left(\phi_d^* - \phi_1\right)}{\left[1 + (n-1)\Gamma_d \Delta t\left\{1 + \left(\phi_d^*/\phi_s\right)^m\right\}\left(\phi_d^* - \phi_1\right)^{(n-1)}/\phi_s^n\right]^{1/(n-1)}} \tag{5.6}$$

for (4.5) with $n > 1$,

The expressions (5.6) are robust solutions of the evolution equations because they represent analytical solutions for ϕ when all the other coefficients in the equations are held constant. Moreover, once ϕ_2 has been determined then eqn (4.6) can be integrated to deduce that

$$\omega_2 = \text{Min}\left[\omega_1 + \frac{1}{\varepsilon_v}\left|\ln\left\{\frac{1-\phi_1}{1-\phi_2}\right\}\right|, 1\right]. \tag{5.7}$$

Also, notice from (5.6) that large values of Γ_c and Γ_d cause ϕ to follow ϕ_c^* during compaction and ϕ_d^* during dilation. On the other hand, the values of Γ_c and Γ_d can be used to match increases in compaction strength and dilation strength that can be observed in high strain rate experiments.

Once the value of ϕ_2 has been determined it is possible to use the expressions (2.18) and (5.4) to obtain the value J_{e2} or J_e. Moreover, the value ε_{s2} of ε_s can be determined by estimating the effect of the mechanical power $\mathbf{T} \cdot \mathbf{D}$ acting in the energy equation during the time step. Then, the value p_2 of p can be determined by the eqns $(2.28)_9$ and (2.32) using the value J_{e2}. Also, the constitutive equations for ε_s can be used to obtain the value θ_2 of the temperature θ.

Next, attention is focused on determining the response to distortional deformation. In this regard, it was shown in (Rubin, 1989; Rubin and Attia, 1996) that the evolution eqn $(2.12)_2$ for elastic distortional deformation with the specifications (2.14) can be integrated numerically over the time step (t_1, t_2) by first calculating an elastic trial stress $\mathbf{T}'^*$ and von Mises stress σ_e^*, such that

$$\mathbf{B}_e'^* = \mathbf{B}_{e1}' + \int_{t_1}^{t_2}\left[\mathbf{L}\mathbf{B}_e' + \mathbf{B}_e'\mathbf{L}^T - \frac{2}{3}(\mathbf{D}\cdot\mathbf{I})\mathbf{B}_e'\right]\mathrm{d}t,$$

$$\mathbf{T}'^* = J_{e2}^{-1}\left(1-\phi_2\right)G(J_{e2}, \theta_1)\mathbf{B}_e''^*, \quad \mathbf{B}_e''^* = \mathbf{B}_e'^* - \frac{1}{3}\left(\mathbf{B}_e'^* \cdot \mathbf{I}\right)\mathbf{I},$$

$$\sigma_e^{*2} = \frac{3}{2}\mathbf{T}'^* \cdot \mathbf{T}'^*. \tag{5.8}$$

Now, the radial return method (Wilkins, 1964) is used to determine values of quantities at the end of the time step

$$\mathbf{B}_{e2}'' = \lambda \mathbf{B}_e''^*, \quad \mathbf{T}_2' = \lambda \mathbf{T}'^*, \quad \sigma_{e2} = \lambda \sigma_e^*. \tag{5.9}$$

Here, λ is a scale factor that is determined by satisfying the evolution eqn $(2.12)_2$ implicitly at the end of

the time step (Rubin, 1989)

$$(1-\lambda) = \Delta t \Gamma_{p2} \lambda, \tag{5.10}$$

where Γ_{p2} is the value of the function Γ_p evaluated at the end of the time step.

For rate-independent plasticity with the yield surface (3.2), plastic deformation rate causes the value of σ_e to remain equal to Y during loading. For this case λ is determined by the conditions (Wilkins, 1964)

$$\lambda = 1 \quad \text{for } \sigma_e^* < Y^*,$$

$$\lambda = \frac{Y^*}{\sigma_e^*} \quad \text{for } \sigma_e^* \geqslant Y^*, \tag{5.11}$$

where Y^* is an estimate of the value of yield strength during the time step. Specifically, since the Lode angle β is unaffected by the magnitude of $\mathbf{T}'$ the value β_2 can be determined using (3.13) with $\mathbf{T}'$ replaced by $\mathbf{T}'^*$. Thus, the estimate Y^* can be specified by

$$Y^* = Y_0 F_1(\varepsilon_{p1}) F_2(p_2) F_3(\Omega_1) F_4(\beta_2) F_5(J_{e2}, \theta_1) F_6(\phi_2) F_7(\omega_2, p_2). \tag{5.12}$$

For general rate-dependent viscoplasticity the eqn (5.10) must be solved iteratively to determine the value of λ. However, when Γ_p is specified by (3.3) and $\sigma_e^* \geqslant Y^*$ then eqn (5.10) becomes a quadratic equation that can be solved analytically for λ. To this end, it is convenient to introduce an auxiliary parameter $\bar{\lambda}$ by the expression

$$\bar{\lambda} = \frac{\lambda \sigma_e^* - Y^*}{Y_0}, \tag{5.13}$$

so that the value of λ is determined by equations

$$d_0 = -1 + \frac{Y^*}{\sigma_e^*}, \quad d_1 = \frac{Y_0}{\sigma_e^*}, \quad d_2 = (\Delta t \Gamma_{p0}) \left[\frac{3G}{\sigma_e^*} \right],$$

$$d_2 \bar{\lambda}^2 + d_1 \bar{\lambda} + d_0 = 0, \quad \bar{\lambda} = \frac{-d_1 + (d_1^2 - 4 d_2 d_0)^{1/2}}{2 d_2},$$

$$\lambda = 1 \quad \text{for } \sigma_e^* \leqslant Y^*, \quad \lambda = \frac{\bar{\lambda} Y_0 + Y^*}{\sigma_e^*} \quad \text{for } \sigma_e^* > Y^*. \tag{5.14}$$

Moreover, it can be shown that when Γ_{p0} is quite large then the solution (5.14) approaches the rate-independent solution (5.11).

Once the value of λ has been determined by either of eqns (5.11) or (5.14), then the deviatoric stress is determined by (5.9) and the equivalent plastic strain ε_p can be updated by using (3.5), (3.6), (5.8) and (5.10) to obtain an expression similar to that developed in (Rubin and Attia, 1996)

$$\varepsilon_{p2} = \varepsilon_{p1} + (1-\lambda) \frac{\sigma_e^*}{3 J_{e2}^{-1} (1-\phi_2) G(J_{e2}, \theta_1)}. \tag{5.15}$$

Then, the value Y_2 of the yield strength can be determined by the eqn (3.7) with this updated value ε_{p2}.

Obviously, different functional forms for hardening $F_1(\varepsilon_p)$ and damage $F_3(\Omega)$ in (3.7) can be used to improve the comparison of the yield strength with experimental data without significant changes in the numerical algorithm.

Next, the value of $\mathbf{B}'_{e2}$ is determined using the equation

$$\mathbf{B}'_{e2} = \mathbf{B}''_{e2} + \tfrac{1}{3}\alpha_{12}\mathbf{I}, \quad \alpha_{12} = \mathbf{B}'_{e2} \cdot \mathbf{I}. \tag{5.16}$$

However, since $\mathbf{B}'_{e2}$ is a unimodular tensor ($\det \mathbf{B}'_{e2} = 1$) it follows that α_{12} becomes the root of the cubic equation

$$\left[\frac{\alpha_{12}}{3}\right]^3 - \frac{1}{2}\left(\mathbf{B}''_{e2} \cdot \mathbf{B}''_{e2}\right)\left[\frac{\alpha_{12}}{3}\right] - \left(1 - \det \mathbf{B}''_{e2}\right) = 0. \tag{5.17}$$

The relevant solution of this equation is given in the appendix of (Rubin and Attia, 1996). Moreover, with the help of (2.29) and (5.10) it can be shown that the rate of material dissipation becomes

$$\rho\theta\xi'_{d2} = \frac{1}{2}(1-\phi_2)J_{e2}^{-1}G\left[\frac{\lambda(1-\lambda)}{\Delta t}\right]\mathbf{B}''^{*}_{e} \cdot \mathbf{B}''^{*}_{e}. \tag{5.18}$$

Finally, using the updated values of pressure and deviatoric stress it is possible to improve the estimate of the internal energy ε_2.

6. Examples

The objective of this section is to present a number of examples which demonstrate the influence of various material constants in the proposed constitutive model. Some of the material constants are applicable to geological type materials while others are applicable to metals. Therefore, it is not possible to explore the influence of all material constants on the response of a single real material. For this reason attention will be focused on two types of materials. Also, some of the material constants for each of these materials are not known from experimental data and are specified here mainly to exhibit the range of material response predicted by the present constitutive model. Moreover, for simplicity the shear modulus G is taken to be constant ($A_1 = A_2 = 0$) and the effect of heat conduction is ignored with k vanishing.

In the examples that follow it is desirable to consider three different types of deformations. To this end, let the vectors $\mathbf{X}$ and $\mathbf{x}$ be referred to a fixed set of rectangular Cartesian base vectors $\mathbf{e}_i$. For pure dilatational deformation the components of these vectors, the velocity gradient $\mathbf{L}$, the total axial Lagrangian strain E_{11} and total volumetric strain E_v are given by

$$\begin{aligned} x_1 &= \exp(D_v t)X_1, \quad x_2 = \exp(D_v t)X_2, \quad x_3 = \exp(D_v t)X_3, \\ \mathbf{L} &= D_v\mathbf{I}, \quad E_{11} = \tfrac{1}{2}\left[\exp(2D_v t) - 1\right], \\ E_v &= J - 1 = \exp(3D_v t) - 1, \end{aligned} \tag{6.1}$$

where $3D_v$ is the constant volumetric deformation rate. For simple shear, which is a purely distortional deformation, the motion and deformation quantities are given by

$$\begin{aligned} x_1 &= X_1 + \kappa t X_2, \quad x_2 = X_2, \quad x_3 = X_3, \\ \mathbf{L} &= \kappa(\mathbf{e}_1 \otimes \mathbf{e}_2), \quad E_{12} = \tfrac{1}{2}\kappa t, \end{aligned} \tag{6.2}$$

where κ is the constant shear rate and E_{12} is the total Lagrangian shear strain. Also, for uniaxial strain, which combines dilatational and distortional deformations, the deformation quantities are given by

$$\begin{aligned} &x_1 = \exp(D_u t)X_1, \quad x_2 = X_2, \quad x_3 = X_3, \\ &\mathbf{L} = D_u(\mathbf{e}_1 \otimes \mathbf{e}_1), \quad E_{11} = \tfrac{1}{2}\left[\exp(2D_u t) - 1\right], \\ &E_v = J - 1 = \exp(D_u t) - 1, \end{aligned} \tag{6.3}$$

where D_u is the constant rate of extension in the $\mathbf{e}_1$ direction and E_{11} is the total Lagrangian axial strain.

The material constants used in the simulations of a geological material and a metal are summarized in Table 2. These constants are used in all simulations except for those where the effect of varying a specific constant are explored. The values of $\{\Phi, \rho_{s0}, C_{s0}, S, \gamma_{s0}\}$ were determined by the work of Heard et al. (1973) on Mt Helen Tuff and Ree (1976) on silicon dioxide and they correspond to the low pressure values that were recorded in (Rubin et al., 1996). Also, the values of $\{G, Y_0, k_3, k_4\}$ were determined by the work of Heard et al. (1973). Figs. 1 and 2 show the response to pure dilatational compaction (6.1) with

$$D_v = \pm 1.0 \times 10^{-3}\mathrm{s}^{-1}. \tag{6.4}$$

For these calculations the values of $\{p_c, c_1, c_2\}$ in Table 2 were determined to provide a best fit with the experimental compaction curve for dry Tuff (Heard et al., 1973). Fig. 1 exhibits the influence of the material constant c_1 and Fig. 2 exhibits the influence of the material constant c_2 on the shape of the

Table 2
Material constants used in the simulations of a geological material and a metal

Parameter	Equation	Geological material	Metal	Parameter	Equation	Geological material	Metal
Φ	(2.16)	0.38	0.0	ε_d	(3.12)	0.5	—
ρ_{s0} (Mg/m^3)	(2.24)	2.32	2.7	Q_{10}	(3.19)	$\sqrt{3}Q_{20}/(1+Q_{20})$	1.0
C_{s0} (km/s)	(2.31)	3.94	5.38	Q_{20}	(3.19)	$3p_d/Y_0$	1.0
S_1	(2.31)	1.98	1.337	q	(3.19)	0.5	—
S_2	(2.31)	0.0	0.0	k_7	(3.22)	0.99	0.99
S_3	(2.31)	0.0	0.0	k_8	(3.22)	1.0	1.0
γ_{s0}	(2.31)	0.69	2.0	ϕ^*	(4.2)	0.01	0.0
b	(2.31)	0.0	0.0	m_d	(4.2)	1.0	0.0
c_{sv}(J/Kg/K)	(2.32)	1.247×10^3	2.1×10^3	p^* (GPa)	(4.2)	0.001	—
θ_0	(2.32)	300.0	300.0	p_c (GPa)	(4.4)	0.03	—
G_0 (GPa)	(2.35)	7.1	29.3	Γ_c (s^{-1})	(4.4)	1.0×10^7	1.0×10^8
$A_1(GPa^{-1})$	(2.35)	0.0	0.0	Γ_d (S^{-1})	(4.5)	3.0×10^3	2.7×10^3
$A_2(K^{-1})$	(2.35)	0.0	0.0	ϕ_s	(4.5)	0.001	0.01
k(J/s/K/m^2)	(2.38)	0.0	0.0	m	(4.5)	12.0	12.8
Γ_{P0} (s^{-1})	(3.3)	∞	1.43×10^6	n	(4.5)	1.0	1.0
							2.0
Y_0 (GPa)	(3.3)	0.08	0.213	ε_v	(4.6)	0.02	0.02
k_1	(3.8)	1.0	1.55	c_1	(4.10)	0.925	—
k_2	(3.8)	—	7.05×10^2	c_2	(4.10)	1.29	—
k_3(GPa^{-1})	(3.9)	10.0	0.0	c_3	(4.10)	0.5	—
k_4(GPa^{-1})	(3.9)	1.3	—	c_4	(4.10)	0.5	—
k_5	(3.10)	0.5	0.0	p_{d0}(GPa)	(4.14)	0.01	0.11
k_6	(3.10)	1.0	—				

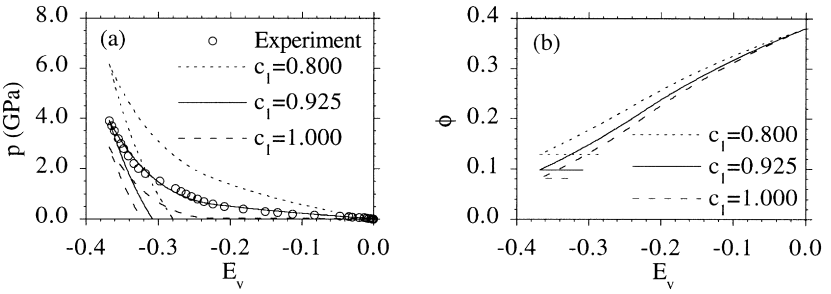

Fig. 1. Pure dilatational compression of a geological material. (a) Comparison of the theoretical compaction curve [for (6.4)] with experimental data for Mt Helen Tuff. (b) Associated values of porosity for the simulations. The influence of changes in the material constant c_1 are also shown.

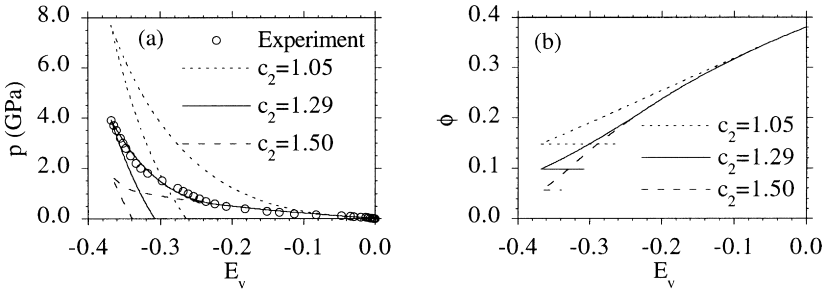

Fig. 2. Pure dilatational compression of a geological material. (a) Comparison of the theoretical compaction curve [for (6.4)] with experimental data for Mt Helen Tuff. (b) Associated values of porosity for the simulations. The influence of changes in the material constant c_2 are also shown.

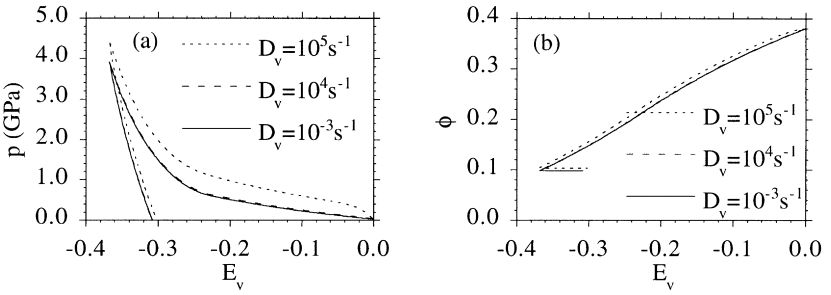

Fig. 3. Pure dilatational compression of a geological material. The curves show the effect of the rate D_v of dilatational compaction.

predicted compaction curves. Moreover, it is noted that the simple model presented here does not exhibit the added elastic compressibility of porosity (that was included in the more complicated model of Rubin et al., 1996) because porosity remains nearly constant during unloading. This causes the elastic loading and unloading curves to be stiffer than the experimental data. Fig. 3 shows that when the deformation rate D_v becomes higher than about $10^4\ s^{-1}$ the model predicts significant rate sensitivity with increased values of pressure and porosity during compaction.

For geological materials the effect of hardening due to distortional deformation has been omitted so that $k_1 = 1$ in Table 2. Fig. 4 compares the response to pure dilatational deformation (6.4) with that to

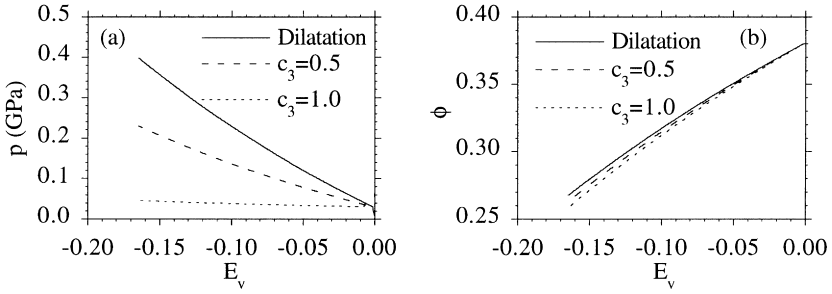

Fig. 4. Comparison of the response of a geological material to pure dilatational compression [for (6.4)] with that to uniaxial strain [for (6.5)] showing the effect of shear enhanced compaction.

uniaxial strain. For these simulations the deformation rate D_u is specified by

$$D_u = \pm 3.0 \times 10^{-3}\ \mathrm{s}^{-1}, \tag{6.5}$$

in order to cause the same volumetric deformation rate (6.4) as that associated with pure dilatational deformation. These figures show that shear enhanced compaction causes the pressure to be lower and the porosity to be smaller for uniaxial strain than for pure dilatational compression. Notice also that for $c_3 = 1$ the effect of shear enhanced compaction is maximized and the response is similar to that predicted by taking $c_1 = 1$, with the pressure remaining nearly constant during compaction. Furthermore, it is noted that the uniaxial response includes a slight pressure increase due to heating associated with plastic distortional deformation which is in addition to the heating associated with porous compaction.

Next, the effect of porous dilation under tension is exhibited. The values of Γ_d, c_d, n in Table 2 cause the porosity to closely follow ϕ_d^* during porous dilation. Fig. 5 shows the response to pure dilatational deformation with D_v given by (6.4). The dotted lines show compaction followed by dilation (cycle abcd) and the solid lines show dilation followed by compaction (cycle aefb). Notice that the magnitude of the pressure at which dilation first occurs in cycle (abcd) is smaller than that in cycle (aefb) because damage due to porosity causes the magnitude of p_d to decrease in cycle (abcd) as the material is compacted. Also, notice that the pressure remains nearly zero during recompression in cycle (aefd) until the porosity attains the value ϕ_{min} then it increases elastically until it reaches the compaction pressure p_c.

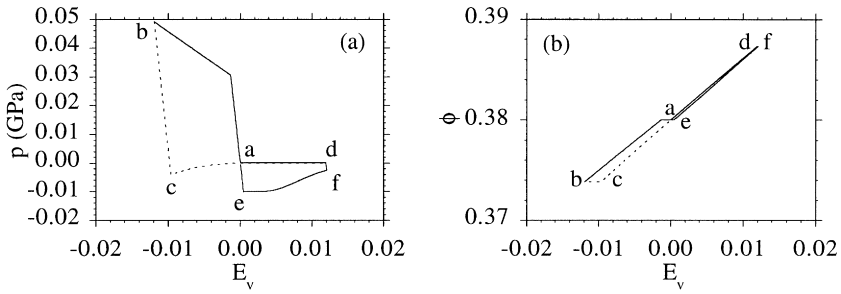

Fig. 5. Cycles of pure dilatational deformation [for (6.4)] of a geological material. The dotted lines show porous compaction followed by dilation (cycle abcd) and the solid lines show dilation followed by compaction (cycle aefb).

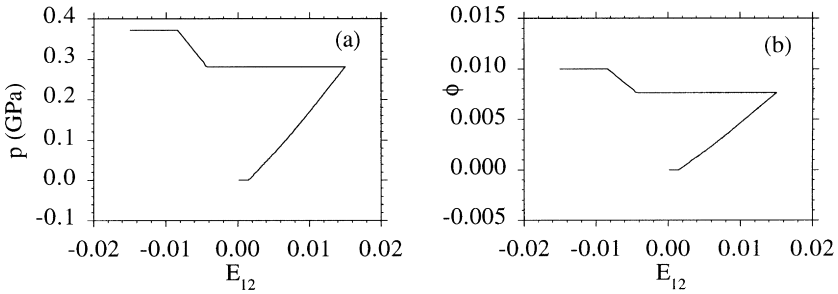

Fig. 6. Cycles of simple shear [for (6.7)] of a geological material (with $\Phi = 0$ and $\gamma_{s0} = 0$) showing the effect of porous dilation due to distortional deformation.

To explore the effect of porous dilation due to distortional deformation (4.2), the same material parameters are used except that Φ is taken to vanish and thermal effects are neglected

$$\Phi = 0, \quad \gamma_{s0} = 0, \tag{6.6}$$

so that the pressure becomes a function of J and ϕ only. Fig. 6 shows the response to a cycle of simple shear with the shear rate specified by

$$\kappa = \pm 1.0 \times 10^{-3}\ \mathrm{s}^{-1}. \tag{6.7}$$

In particular, notice that even though the volume remains constant during simple shear, both the pressure and the porosity increase due to distortional deformation.

Fig. 7 shows the same effect occurring in a cycle of uniaxial compression with D_u given by (6.5). For comparison, Fig. 7 also shows the response for the value $\phi^* = 0.2$ since the experiments of (Glenn et al., 1990) on glass indicated increases in porosity up to 0.2 after shock loading. Fig. 7(a) shows that the pressure upon unloading is higher than that upon loading because porous dilation during loading is caused by distortional deformation. This is a similar response to that predicted by the model of Glenn et al. (1990). For $\phi^* = 0.01$ the porosity saturates at the value $\phi = 0.01$ and then the material unloads elastically until the pressure reaches the value $(-p_d)$ at which time dilation occurs due to negative pressure. However, for $\phi^* = 0.2$ the porosity continues to dilate during unloading at positive pressure since for this range of strain ϕ remains smaller than ϕ^*. Although Fig. 7(a) indicates that the pressure

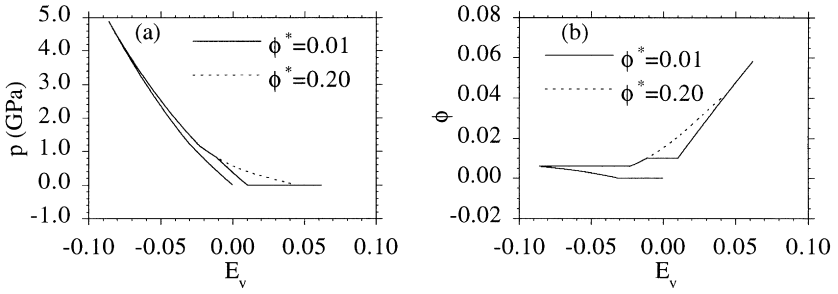

Fig. 7. A cycle of uniaxial compression [for (6.5)] of a geological material (with $\Phi = 0$ and $\gamma_{s0} = 0$) showing porous dilation due to distortional deformation for two values of ϕ^*.

does negative work in the cycle, it should be remembered that the second law of thermodynamics (2.37) ensures that the dissipation due to distortional deformation compensates this negative work.

For metals it is common to consider a simple form for the yield strength that ignores the effects of pressure hardening, distortional damage and the Lode angle, which leads to the values of $\{k_1, k_3, k_5, Q_{10}, Q_{20}\}$ given in Table 2. Also the initial porosity is assumed to vanish and the effect of porous dilation due to distortional deformation is eliminated, which yields the values of $\{\Phi, \phi^*\}$. Next, using the work in Rubin (1990) it can be shown that

$$\Gamma_{p0} = \left[\frac{2\sqrt{2}}{9}\right] A' Y_0^2, \quad k_1 = \frac{Y_1'}{Y_0}, \quad k_2 = \frac{\dfrac{3K}{2Y_0}}{\dfrac{Y_1'}{Y_0} - 1}, \tag{6.8}$$

where $\{A', Y_0, Y_1', K\}$ are constants that are given in Swegle and Grady (1985) (here, for clarity the symbol Y_1' is used instead of Y_1 in their paper). Moreover, in their work (Swegle and Grady, 1985) values for these constants as well as for $\{\rho_{s0}, C_{s0}, S_1, \gamma_{s0}\}$ and Poisson's ratio v are given for a number of materials with the shear modulus G_0 being approximated by the expression

$$G_0 = \frac{3\rho_{s0}C_{s0}^2(1-2v)}{2(1+v)}. \tag{6.9}$$

The values of these constants for aluminum are specified in Table 2.

Fig. 8 shows the response of aluminum to cycles of loading and unloading in simple shear at different shearing rates κ. Notice that the viscoplastic response causes the flow stress to increase with increased shearing rate.

To simulate static tensile failure the parameter p_{d0} was taken to be about one third of the maximum yield strength. Moreover, given a value for the parameter n in (4.5) the parameters $\{\Gamma_d, m\}$ were determined by matching the peak values of tension T_{11} during spallation at various constant uniaxial strain rates D_u with an empirical formula for spall stress σ^* which fits experimental data (Kanel et al., 1997)

$$\sigma^* = 0.635(D_u)^{0.059} \text{ GPa}, \tag{6.10}$$

where D_u is measured in sec^{-1}. The values of these parameters associated with $n = 1$ are given in Table 2 and the values associated with $n = 2$ are given by

$$\Gamma_d = 2.24 \times 10^3 \text{ s}^{-1}, \quad m = 12.0, \quad n = 2. \tag{6.11}$$

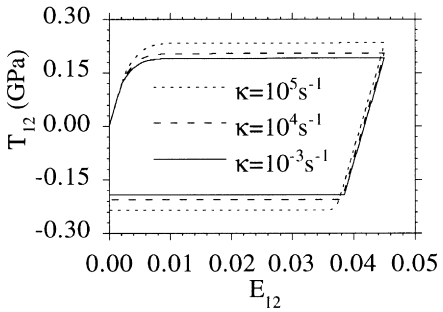

Fig. 8. Cycles of simple shear [for (6.7)] of aluminum at different shearing rates κ.

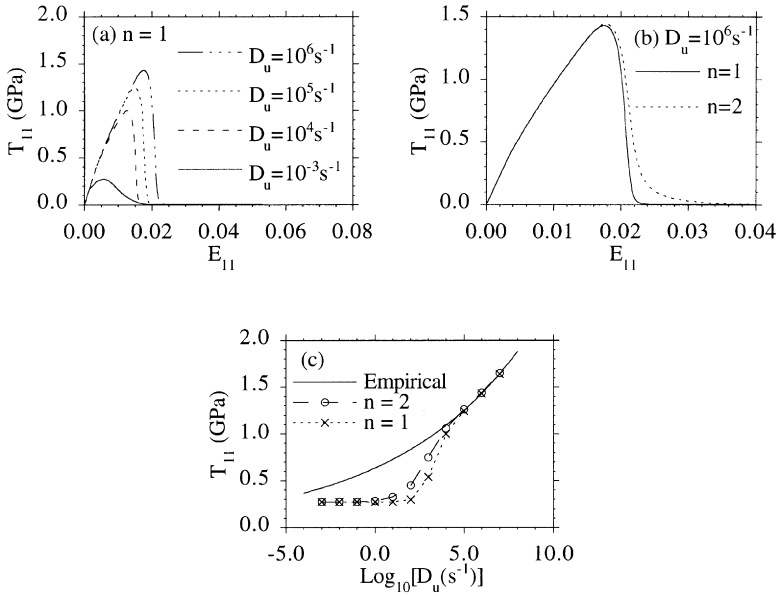

Fig. 9. Uniaxial expansion of aluminum. (a) The effect of different rates D_u for $n = 1$. (b) The effect of changing the value of n. (c) Comparison of the theoretical peak values of tension T_{11} with the empirical formula (6.10) for two values of n.

Fig. 9(a) (associated with $n = 1$) shows the response of aluminum to uniaxial strain at different expansion rates D_u and indicates a rate-dependent peak spall strength as well as a rapid drop in strength once spallation becomes significant. Fig. 9(b) shows the response for $D_u = 10^6\ s^{-1}$ and indicates that increasing the value of n causes the spall stress to decrease more slowly. Also, Fig. 9(c) shows that both sets of parameters $\{\Gamma_d, m, n\}$ match the empirical formula fairly well in the usual range of spall experiments ($D_u = 10^4$–$10^6\ s^{-1}$) and that both yield the same quasi-static value of spall strength. Moreover, this figure suggests that the value of n can be determined by matching the value of strain rate associated with the onset of the rapid increase in spall strength.

In summary, the examples presented in this section show that the constitutive equations discussed in this paper can model a wide range of material response which include both dry porous geological materials and nonporous and porous metals.

Acknowledgements

This research was performed under the auspices of the U.S. Department of Energy by Lawrence Livermore National Laboratory under contract No. W-7405-Eng-48 and M.B. Rubin was partially supported by the Fund for Promotion of Research at Technion. Also, the authors would like to acknowledge helpful discussions with Dr I.N. Lomov and Mr J.U. Cazamias related to the revised version of the paper.

References

Besseling, J.F., 1966. A thermodynamic approach to rheology. In: Parkus, H., Sedov, L.I. (Eds.), Proc. of the IUTAM Symposium on Irreversible Aspects of Continuum Mechanics and Transfer of Physical Characteristics in Moving Fluids, Vienna. Springer-Verlag, Wein, 1968, pp. 16–53.

Bodner, S.R., 1987. Review of a unified elastic–viscoplastic theory. In: Miller, A.K. (Ed.), Unified Constitutive Equations for Creep and Plasticity. Elsevier, UK.

Bodner, S.R., Partom, Y., 1972. A large deformation elastic–viscoplastic analysis of a thick-walled spherical shell. ASME J. Appl. Mech. 39, 751–757.

Carroll, M., Holt, A.C., 1972. Suggested modification of the P–α model for porous materials. J. Appl. Phys. 43, 759–761.

Chen, W.F., Baladi, G.Y., 1985. Soil Plasticity, Theory and Implementation. Elsevier, Amsterdam.

Curran, D.R., Seaman, L., Shockey, D.A., 1987. Dynamic failure of solids. Physics Reports (A Review Section of Physics Letters) 147, 253–388.

Eckart, C., 1948. The thermodynamics of irreversible processes. IV. The theory of elasticity and anelasticity. Physical Review 73, 373–382.

Flory, P.J., 1961. Thermodynamic relations for high elastic materials. Trans. Faraday Soc. 57, 829–838.

Glenn, L.A., Moran, B., Kusubov, A.S., 1990. Modeling jet penetration in glass. Conference on the Application of 3-D Hydrocodes to Armor/Anti-Armor Problems, BRL, Aberdeen Proving Grounds, MD, 8–9 May 1990; also, Report UCRL-JC-103512, Lawrence Livermore National Laboratory, Livermore, CA.

Green, A.E., Naghdi, P.M., 1977. On thermodynamics and the nature of the second law. Proc. R. Soc. Lond. A357, 253–270.

Green, A.E., Naghdi, P.M., 1978. The second law of thermodynamics and cyclic processes. ASME J. Appl. Mech. 45, 487–492.

Gurson, A.L., 1977. Continuum theory of ductile rupture by void nucleation and growth: Part 1—yield criteria and flow rules for porous ductile media. ASME J. Eng. Mater. Technol. 99, 2–15.

Heard, H.C., Bonner, B.P., Duba, A.G., Hock, R.N., Stephens, D.R., 1973. High Pressure Mechanical Properties of Mt Helen, Nevada, Tuff. Report No. UCID-16261, Lawrence Livermore National Laboratory, Livermore, CA.

Hill, R., 1950. The Mathematical Theory of Plasticity. Oxford University Press, London.

Johnson, J.N., Addessio, F.L., 1988. Tensile plasticity and ductile fracture. J. Appl. Phys. 64, 6699–6712.

Kanel, G.I., Razorenov, S.V., Bogatch, A., Utkin, A.V., Grady, D.E., 1997. Simulation of spall fracture of aluminum and magnesium over a wide range of load duration and temperature. Int. J. Impact Engng. 20, 467–478.

Leonov, A.I., 1976. Nonequilibrium thermodynamics and rheology of viscoelastic polymer media. Rheologica Acta 15, 85–98.

Ree, F.H., 1976. Equation of State of the Silicon Dioxide System. Report No. UCRL-52153, Lawrence Livermore National Laboratory, Livermore, CA.

Rubin, M.B., 1986. An elastic–viscoplastic model for large deformation. Int. J. of Eng. Sci. 24, 1083–1095.

Rubin, M.B., 1987a. An elastic–viscoplastic model for metals subjected to high compression. ASME J. Appl. Mech. 54, 532–538.

Rubin, M.B., 1987b. An elastic–viscoplastic model exhibiting continuity of solid and fluid states. Int. J. of Engng. Sci 25, 1175–1191.

Rubin, M.B., 1989. A time integration procedure for large plastic deformation in elastic–viscoplastic metals. Journal of Mathematics and Physics (ZAMP) 40, 846–871.

Rubin, M.B., 1990. Efficient time integration of a viscoplastic model for shock waves. J. Appl. Phys. 68, 1356–1358.

Rubin, M.B., 1991. A simple and convenient isotropic failure surface. ASCE J. Engineering Mechanics 117, 348–369.

Rubin, M.B., 1994. Plasticity theory formulated in terms of physically based microstructural variables—Part I: theory. Int. J. Solids Structures 31, 2615–2634.

Rubin, M.B., 1996. On the treatment of elastic deformation in finite elastic–viscoplastic theory. Int. J. Plasticity 12, 951–965.

Rubin, M.B., Attia, A.V., 1990. A Continuum Tensile Failure Model with Friction. UCRL-ID-104759, Lawrence Livermore National Laboratory, Livermore, CA, August.

Rubin, M.B., Attia, A., 1996. Calculation of hyperelastic response of finitely deformed elastic–viscoplastic materials. Int. J. Numerical Meth. Engng. 39, 309–320.

Rubin, M.B., Chen, R., 1991. Universal relations for elastically isotropic elastic–plastic materials. ASME J. Appl. Mech. 58, 283–285.

Rubin, M.B., Yarin, A.L., 1993. On the relationship between phenomenological models for elastic–viscoplastic metals and polymeric liquids. J. Non-Newtonian Fluid Mech. 50, 79–88. Corrigendum, 1995, 57, 321.

Rubin, M.B., Elata, D., Attia, A.V., 1996. Modeling added compressibility of porosity and the thermomechanical response of wet porous rock with application to Mt Helen Tuff. Int. J. Solids Structures 33, 761–793.

Steinberg, D.J., 1991. Equation of State and Strength Properties of Selected Materials. Report No. UCRL-MA-106439, Lawrence Livermore National Laboratory.

Steinberg, D.J., Cochran, S.G., Guinan, M.W., 1980. A constitutive model for metals applicable at high-strain rates. J. Appl. Phys. 51, 1498–1504.

Swegle, J.W., Grady, D.E., 1985. Shock viscosity and the prediction of shock wave rise times. J. Appl. Phys. 58, 692–701.

Swegle, J.W., Grady, D.E., 1986. Shock viscosity and the calculation of steady shock wave profiles. In: Gupta, Y.M. (Ed.), Shock Waves in Condensed Matter. Plenum, New York, pp. 353–357.

Wilkins, M.L., 1964. Calculation of elastic–plastic flow. In: Methods in Computational Physics, vol. 3. Academic Press, New York, pp. 211–263.